NAVAL POSTGRADUATE SCHOOL

MONTEREY, CALIFORNIA

THESIS

ANALYSIS AND SIMULATION OF DISADVANTAGED RECEIVERS FOR MULTIPLE-INPUT MULTIPLE-OUTPUT COMMUNICATIONS SYSTEMS

by

Tracy A. Martin

September 2010

Thesis Advisor:	Frank Kragh
Second Reader:	Tri Ha

Approved for public release; distribution is unlimited

THIS PAGE INTENTIONALLY LEFT BLANK

REPORT DOCUMENTATION PAGE		Form Approved OMB No. 0704-0188

1. AGENCY USE ONLY *(Leave blank)*	2. REPORT DATE September 2010	3. REPORT TYPE AND DATES COVERED Master's Thesis

4. TITLE AND SUBTITLE Analysis and Simulation of Disadvantaged Receivers for Multiple-Input Multiple-Output Communications Systems	5. FUNDING NUMBERS
6. AUTHOR(S) Tracy A. Martin	
7. PERFORMING ORGANIZATION NAME(S) AND ADDRESS(ES) Naval Postgraduate School Monterey, CA 93943-5000	8. PERFORMING ORGANIZATION REPORT NUMBER
9. SPONSORING /MONITORING AGENCY NAME(S) AND ADDRESS(ES) N/A	10. SPONSORING/MONITORING AGENCY REPORT NUMBER

11. SUPPLEMENTARY NOTES The views expressed in this thesis are those of the author and do not reflect the official policy or position of the Department of Defense or the U.S. Government. IRB Protocol number _____N/A_____.

12a. DISTRIBUTION / AVAILABILITY STATEMENT Approved for public release; distribution is unlimited	12b. DISTRIBUTION CODE

13. ABSTRACT (maximum 200 words)

This thesis investigates the simulation performance of Multiple-Input Multiple-Output (MIMO) communication systems. Uncoded narrowband and wideband MIMO systems are presented and simulated. The system is further refined with the addition of Space-Time Codes (STC) and Channel State Information at the Transmitter (CSIT). A disadvantaged receiver is subsequently introduced to the system lacking the optimization enjoyed by the native receiver. Simulation and analysis was conducted with multiple modulation schemes and antenna configurations. Rayleigh and Rician fading models are developed and simulated as the wireless channel. Receiver performance results based on MATLAB simulation are compared and presented.

14. SUBJECT TERMS Multiple-Input Multiple-Output (MIMO), Orthogonal Frequency Division Multiplexing (OFDM), Binary Phase Shift Keying, Quadrature Phase Shift Keying, Quadrature Amplitude Modulation, Rayleigh Fading Channel, Rician Fading Channel, Space-Time Code (STC), Disadvantaged Receiver, Linear Diversity Precoding, Channel State Information (CSI)	15. NUMBER OF PAGES 106
	16. PRICE CODE

17. SECURITY CLASSIFICATION OF REPORT	18. SECURITY CLASSIFICATION OF THIS PAGE	19. SECURITY CLASSIFICATION OF ABSTRACT	20. LIMITATION OF ABSTRACT
Unclassified	Unclassified	Unclassified	UU

NSN 7540-01-280-5500 Standard Form 298 (Rev. 2-89)
Prescribed by ANSI Std. 239-18

THIS PAGE INTENTIONALLY LEFT BLANK

Approved for public release; distribution is unlimited

ANALYSIS AND SIMULATION OF DISADVANTAGED RECEIVERS FOR MULTIPLE-INPUT MULTIPLE-OUTPUT COMMUNICATIONS SYSTEMS

Tracy A. Martin
Captain, United States Marine Corps
B.S., United States Naval Academy, 2004

Submitted in partial fulfillment of the
requirements for the degree of

MASTER OF SCIENCE IN ELECTRICAL ENGINEERING

from the

NAVAL POSTGRADUATE SCHOOL
September 2010

Author: Tracy A. Martin

Approved by: Frank Kragh
Thesis Advisor

Tri Ha
Second Reader

R. Clark Robertson
Chairman, Department of Electrical and Computer Engineering

THIS PAGE INTENTIONALLY LEFT BLANK

ABSTRACT

This thesis investigates the simulation performance of Multiple-Input Multiple-Output (MIMO) communication systems. Uncoded narrowband and wideband MIMO systems are presented and simulated. The system is further refined with the addition of Space-Time Codes (STC) and Channel State Information at the Transmitter (CSIT). A disadvantaged receiver is subsequently introduced to the system lacking the optimization enjoyed by the native receiver. Simulation and analysis was conducted with multiple modulation schemes and antenna configurations. Rayleigh and Rician fading models are developed and simulated as the wireless channel. Receiver performance results based on MATLAB simulation are compared and presented.

THIS PAGE INTENTIONALLY LEFT BLANK

TABLE OF CONTENTS

LIST OF FIGURES

LIST OF TABLES

THIS PAGE INTENTIONALLY LEFT BLANK

LIST OF ACRONYMS AND ABBREVIATIONS

A/D	Analog to Digital
AWGN	Additive White Gaussian Noise
BER	Bit Error Rate
BPSK	Binary Phase-Shift Keying
CDF	Cumulative Distribution Function
CP	Cyclic Prefix
CSI	Channel State Information
CSIR	Channel State Information at the Receiver
CSIT	Channel State Information at the Transmitter
D/A	Digital to Analog
DFT	Discrete Fourier Transform
FFT	Fast Fourier Transform
IDFT	Inverse Discrete Fourier Transform
IFFT	Inverse Fast Fourier Transform
IID	Independent Identically Distributed
ISI	Intersymbol Interference
LOS	Line of Sight
NLOS	Non-Line of Sight
ML	Maximum Likelihood
MIMO	Multiple-Input Multiple-Output
MISO	Multiple-Input Single-Output
OFDM	Orthogonal Frequency Division Multiplexing
PSD	Power Spectral Density

PDF	Probability Density Function
QAM	Quadrature Amplitude Modulation
QPSK	Quadrature Phase-Shift Keying
RF	Radio Frequency
SISO	Single-Input Single-Output
SNR	Signal to Noise Ratio
STC	Space-Time Code
SVD	Singular Value Decomposition
WSS	Wide-Sense Stationary

EXECUTIVE SUMMARY

Multiple-Input Multiple-Output (MIMO) communications systems are fundamentally different from earlier wireless systems. In MIMO systems, multiple antennas are used for transmission and reception, thus multiple communication paths or channels are developed. These channels can then be utilized to increase the data rate or reliability of the system. Data rate is increased by sending different symbols over multiple channels at the same time. On the other hand, reliability is increased by sending multiple copies of the same symbol, or similar redundancy, over the multiple channels.

This ability of MIMO systems to provide increased reliability and data rate without requiring an increase in bandwidth or power has resulted in MIMO schemes being adopted in standards such as IEEE 802.11n, IEEE 802.16, and Long Term Evolution (LTE) systems, representing most of the WLAN, WMAN, and 4G mobile telephone industry [1]. Our adversaries use conventional wireless devices, and we can expect them to use these MIMO devices also, as they grow in market dominance. We benefit from a thorough understanding of our adversaries' tools. Furthermore, MIMO systems have the potential to greatly improve signal reception and reliability for friendly forces. As the military continues to develop and further rely on high data rate, highly mobile communications, signal reception and reliability is often found to be the weakest link. Mobile networking, in particular, relies heavily on reliable delivery, otherwise routing protocols degenerate and retransmissions swamp the network. By developing and utilizing a robust MIMO system, decision makers can be assured that timely and critical communications will get through. This work seeks to expand that understanding.

Specifically, this thesis evaluates the bit error rate performance of various MIMO system configurations into which a second, disadvantaged receiver is introduced. The analysis begins with a basic two transmit and two receive antenna MIMO system utilizing maximum likelihood decoding. The system is simulated in MATLAB employing BPSK, QPSK, 16QAM and 64QAM over both Rician and Rayleigh channel models in order to demonstrate and analyze the bit error rate performance. The system is improved with the application of the Alamouti space-time coding scheme and simulated.

A comparison of the uncoded and coded systems is conducted. Specifically, when comparing a 2x2 MIMO system utilizing QPSK to that of Alamouti space time coded 2x2 MIMO system utilizing QPSK, we see that the coded system provides the same performance while requiring 10 dB less power. The performance improvement seen is due to the diversity gain provided by the Alamouti scheme. Additionally, the orthogonality of the coding sequence transforms the decision at the receiver from a vector operation into a scalar operation, reducing the receiver complexity.

Next, the system is further refined with the addition of channel state information at the transmitter. This information allows the transmitter to optimize its transmission according to the channel conditions, further improving bit error performance. Results show that a system with channel state information needs 12 dB less power than the equivalent uncoded system for equal performance. In addition, knowledge of the channel provides the receiver with an array gain equal to 2 dB, resulting in increased performance over that of the space-time coded system without channel state information.

Into this robust system, a second receiver is introduced that does not enjoy the same optimization as the intended receiver. This would be important whenever there are multiple receivers attempting to receive the same transmission at distinct locations, as might be the desired configuration in a wireless network employing broadcast transmissions. The performance was evaluated over both Rayleigh and Rician fading channels with various antenna configurations. In the case of a Rayleigh channel, when the number of receive antennas is increased to eight, the performance is 3 dB worse than the intended receiver. In a Rician channel, where the line of sight path has equal power to that of the scattered paths, results show that when the receiver employs four antennas the performance increases to 2 dB better than the intended receiver. Finally, when the disadvantaged receiver is simulated at a location receiving more signal power via line of sight from the transmitter with two receive antennas, the second receiver performs as well as the intended receiver. Thus, depending on the configuration of the disadvantaged receiver it can achieve an equal or superior bit error rate performance than the intended receiver.

ACKNOWLEDGMENTS

I would like to thank my advisor, Professor Frank Kragh, for his guidance and support during the development of this thesis.

THIS PAGE INTENTIONALLY LEFT BLANK

I. INTRODUCTION

A. BACKGROUND

Multiple-input Multiple-output (MIMO) communications systems are fundamentally different from earlier wireless systems. As their name implies, MIMO systems are designed to have additional antennas at the transmitter and receiver, providing spatial diversity not available to single antenna systems. Thus, information can be sent and received over multiple channels.

This gives the communications engineer greater opportunity for robust system designs. One such example is the capability of a MIMO system to transmit at a higher rate and more reliably by using the stronger (less faded) channels more and the weaker (more faded) channels less. As it is discussed in this thesis, that implies the transmission is optimized for the location of one receiver, which is unfortunate in the case of broadcast transmissions. This research seeks to determine how a second receiver would perform given that the transmission is optimized for the location of the first receiver.

B. OBJECTIVES AND METHODOLOGY

The goal of this work was to investigate the performance of a second receiver when presented into an existing MIMO system optimized for the first receiver. The research approach takes a basic system, integrates techniques to improve performance and concludes with the introduction of a second receiver into the system.

Development begins with the simulation of a simple uncoded narrowband MIMO system over Rician and Rayleigh fading channels. To which the Alamouti space-time coding scheme is applied and simulated. Then, the application of Orthogonal Frequency Division Multiplexing (OFDM) is investigated. The system is completed by introducing Channel State Information at the Transmitter (CSIT), where the result is a more robust communications link. Finally, a second receiver is introduced to the optimized system and the performance is simulated. Various scenarios are then investigated in an effort to improve the disadvantaged receiver performance.

C. BENEFITS OF STUDY

MIMO systems are becoming increasingly commonplace, including IEEE 802.11n, IEEE 802.16, and Long Term Evolution (LTE) systems, which represent most of the WLAN, WMAN, and 4G mobile telephone industry [1]. Our adversaries use conventional wireless devices, and we can expect them to use these MIMO devices also, as they grow in market dominance. We benefit from a thorough understanding of our adversaries' tools. This work seeks to expand that understanding. Furthermore, MIMO systems have the potential to greatly improve signal reception and reliability for friendly forces. As the military continues to develop and further rely on high data rate, highly mobile communications, signal reception and reliability is often found to be the weakest link. Mobile networking, in particular, relies heavily on reliable delivery, otherwise routing protocols degenerate and retransmissions swamp the network. By developing and utilizing a robust MIMO system, it is highly likely that timely and critical communications will get through.

D. ORGANIZATION

The thesis is organized into five chapters. Chapter II introduces the MIMO system. It provides a brief background into methods used throughout the thesis. These include channel models, OFDM-MIMO, maximum likelihood (ML) detection, space time coding and channel state information. Chapter III discusses the analysis and simulation of MIMO receivers that involve various configurations of the methods introduced in the previous chapter. Chapter IV examines each of these configurations and provides a comparison of the results. Chapter V provides a summary and gives recommendations for future study.

II. OVERVIEW OF MIMO COMMUNICATIONS

This chapter provides background on the techniques used in designing and analyzing MIMO systems. Specifically, this chapter introduces a lowpass equivalent MIMO system model upon which the remaining topics will build. Rayleigh and Rician fading channels are then discussed, providing a framework for future analysis. Next, OFDM implementation utilizing the Discrete Fourier Transform (DFT) is presented. Maximum Likelihood (ML) detection at the receiver is introduced. Then, space-time codes are developed using the Alamouti scheme. Finally, channel state information is defined for application at the transmitter.

A. LOWPASS EQUIVALENCY

Wireless channels often have different spectral characteristics than that of the information signal. Therefore, before entering the channel it is often necessary to match the spectral characteristics of the signal to that of the channel. In other words, the information signal is at baseband, a lower frequency, and needs to be converted to passband, a higher frequency for transmission. At the receiver, the reverse takes place, converting from passband to baseband. Thus, when analyzing or designing communication systems it is common practice to represent the system in lowpass equivalent form. Representing the system in this manner greatly simplifies analysis since the dependency on the carrier frequency is eliminated. Additionally, signal processing limitations require that we manipulate the information signal at lower frequencies in order to maintain reasonable sampling rates. This section will develop an equivalent lowpass form for bandpass signals [2], [3].

Given a bandpass signal $g(t)$, whose Fourier transform is $G(f)$, then the analytic signal is defined as [2]

$$g_+(t) = g(t) + j\hat{g}(t) \tag{2.1}$$

where $g_+(t)$ denotes only positive frequency components are present and $\hat{g}(t)$ represents the Hilbert Transform of $g(t)$, i.e., $\hat{g}(t) = \frac{1}{\pi t} * g(t)$, where the asterisk denotes convolution.

Taking the Fourier transform of Equation (2.1) yields [1]

$$G_+(f) = G(f) + j\left(-j\,\mathrm{sgn}(f)G(f)\right). \tag{2.2}$$

Equation (2.2) can be simplified by using the property, $\mathrm{sgn}(f) = 2u(f) - 1$, where $u(f)$ is the unit step function, to get

$$G_+(f) = 2G(f)u(f) \tag{2.3}$$

From Equation (2.3) it is clear that the analytic signal represents the bandpass signal at twice the amplitude and consisting of positive frequencies only. Next, let the lowpass equivalent of $g(t)$, denoted as $g_l(t)$, be defined as [2]

$$g_l(t) = g_+(t)e^{-j2\pi f_c t} \tag{2.4}$$

Taking the Fourier transform and substituting Equation (2.3) results in

$$G_l(f) = 2G(f + f_c)u(f + f_c) \tag{2.5}$$

Equation (2.5) shows in the frequency domain, the lowpass equivalent signal or complex envelope is just a scaled and shifted version of the components of the bandpass signal that have positive frequencies. The positive frequency components contain all the information necessary to reconstruct the original signal. In this case, it is scaled by two and shifted from the carrier frequency to the zero frequency or baseband. This result is illustrated in Figure 1.

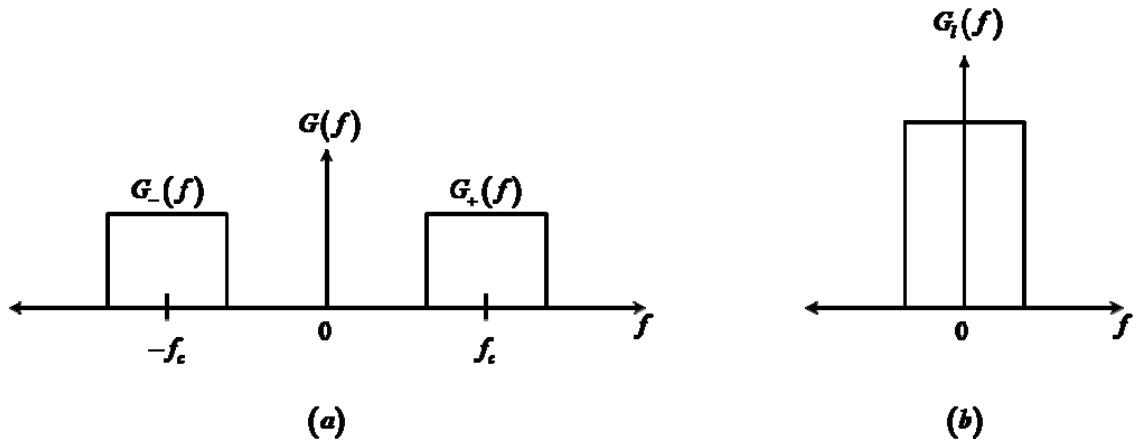

Figure 1. A bandpass signal (a) and the lowpass equivalent (b) (After [2]).

In the time domain

$$g_l(t) = \left(g(t) + j\hat{g}(t)\right)e^{-j2\pi f_c t}. \tag{2.6}$$

Rearranging and isolating the real part of Equation (2.6) produces a representation of a bandpass signal in terms of its lowpass equivalent [2]

$$g(t) = \mathrm{Re}\left[g_l(t)e^{j2\pi f_c t}\right]. \tag{2.7}$$

Additionally, the lowpass equivalent signal can be represented by the in-phase and quadrature components of the baseband signal as [2]

$$g_l(t) = g_i(t) + jg_q(t). \tag{2.8}$$

Substituting Equation (2.8) into Equation (2.6) yields [2]

$$\begin{aligned} g_i(t) &= g(t)\cos(2\pi f_c t) + \hat{g}(t)\sin(2\pi f_c t) \text{ and} \\ g_q(t) &= \hat{g}(t)\cos(2\pi f_c t) - g(t)\sin(2\pi f_c t). \end{aligned} \tag{2.9}$$

Solving for $g(t)$ and $\hat{g}(t)$ yields [2]

$$\begin{aligned} g(t) &= g_i(t)\cos(2\pi f_c t) - g_q(t)\sin(2\pi f_c t) \\ \hat{g}(t) &= g_q(t)\cos(2\pi f_c t) + g_i(t)\sin(2\pi f_c t) \end{aligned} \tag{2.10}$$

or, in polar form, [2]

$$g(t) = r_g(t)\cos\left(2\pi f_c t + \theta_g(t)\right) \tag{2.11}$$

where $r_g(t)$ and $\theta_g(t)$ represent the envelope and phase of $g(t)$.

Thus, we observe that Equation (2.10) defines the modulation process while Equation (2.9) defines the demodulation process and original signal can be completely described in lowpass equivalent form given by Equation (2.7). This conclusion is shown in Figure 2. [2].

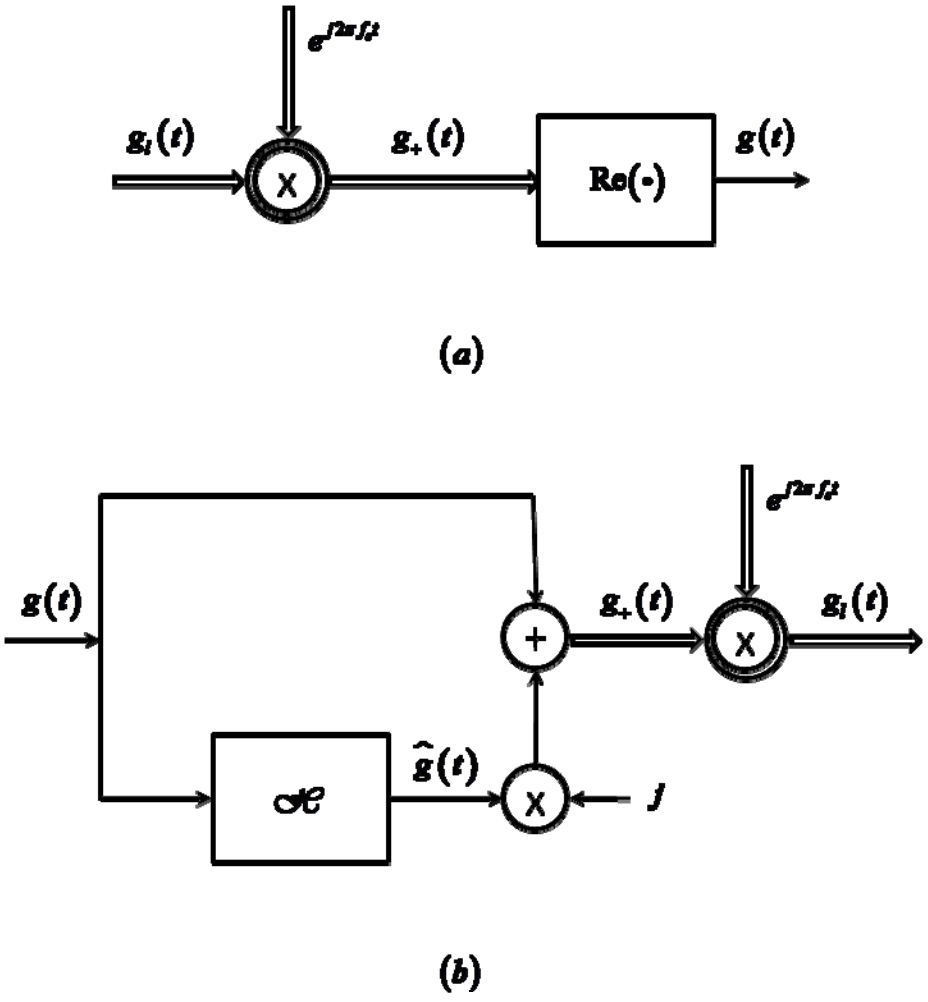

Figure 2. A modulator (a) and demodulator (b) (After [2]).

Next, we develop how the energy of the signal is represented when the signal is expressed in lowpass equivalent form.

Given that the energy of a signal $g(t)$ is defined as [2]

$$\mathrm{E}_g = \int_{-\infty}^{\infty} |g(t)|^2 dt \tag{2.12}$$

applying Parseval's Theorem yields [2]

$$\mathrm{E}_g = \int_{-\infty}^{\infty} |g(t)|^2 dt = \int_{-\infty}^{\infty} |G(f)|^2 df. \tag{2.13}$$

Since $G(f) = G_+(f) + G_-(f)$ and $G_+(f)G_-(f) = 0$ then [2]

$$\begin{aligned} \mathrm{E}_g &= \int_{-\infty}^{\infty} |G_+(f) + G_-(f)|^2 df \\ &= \int_{-\infty}^{\infty} |G_+(f)|^2 df + \int_{-\infty}^{\infty} |G_-(f)|^2 df \\ &= 2\int_{-\infty}^{\infty} |G_+(f)|^2 df \\ &= 2\int_{-\infty}^{\infty} \left|\frac{G_l(f)}{2}\right|^2 df \\ &= \frac{1}{2}\mathrm{E}_{g_l}. \end{aligned} \tag{2.14}$$

This result confirms Equation (2.5): the energy of the lowpass equivalent signal is double that in the bandpass signal. In the remaining analysis, signals and systems will be represented by their lowpass equivalent form.

B. THE MIMO SYSTEM MODEL

A MIMO system comprised of N_T spatially separated transmit antennas and N_R spatially separated receive antennas is depicted in Figure 3.

At the transmitter, the symbol transmitted on antenna n is denoted $s_n(t)$, where $n = 1, 2, ..., N_T$ and t denotes the time variable. The equivalent lowpass channel impulse response between the receive antenna m, and the transmit antenna n, is denoted as $h_{mn}(\tau; t)$. Where τ denotes the delay variable.

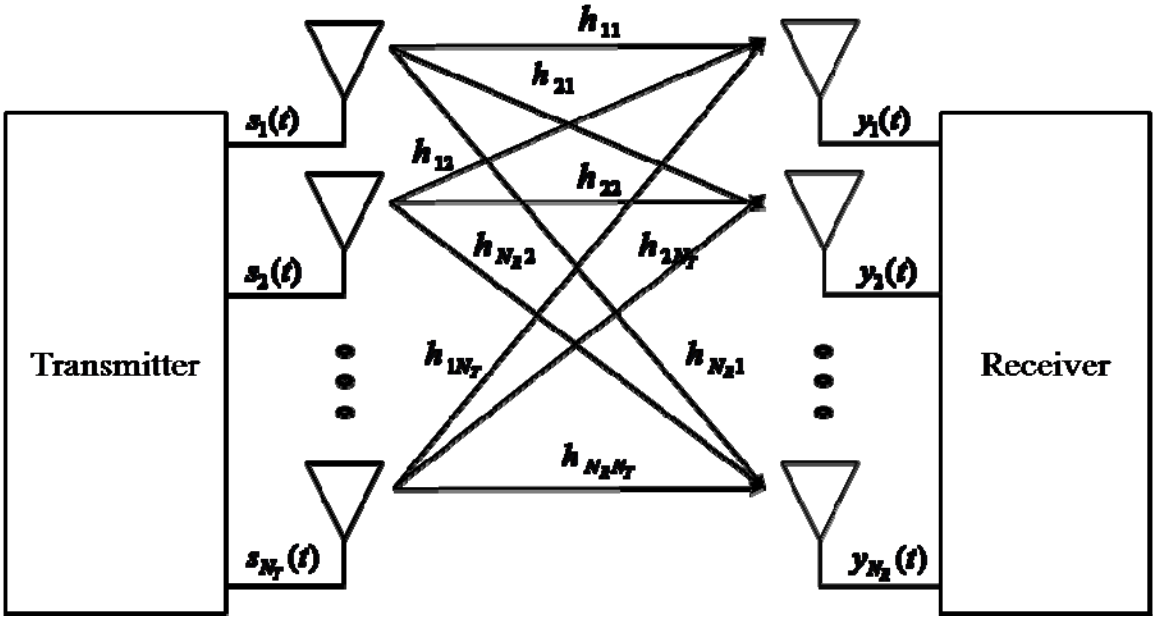

Figure 3. MIMO System Block Diagram (After [2],[3]).

The composite of the complex channel gains is then given by the $N_R \times N_T$ matrix, $\mathbf{H}(\tau;t)$ which is also known as the channel matrix [2]

$$\mathbf{H}(\tau;t) = \begin{bmatrix} h_{11}(\tau;t) & h_{12}(\tau;t) & \cdots & h_{1N_T}(\tau;t) \\ h_{21}(\tau;t) & h_{22}(\tau;t) & \cdots & h_{2N_T}(\tau;t) \\ \vdots & \vdots & \ddots & \vdots \\ h_{N_R2}(\tau;t) & h_{N_R2}(\tau;t) & \cdots & h_{N_RN_T}(\tau;t) \end{bmatrix}. \tag{2.15}$$

The channel matrix is often described with statistical models that accurately predict channel characteristics. This thesis will focus on Rayleigh and Rician fading models, discussed in the next chapter.

The signal at the m^{th} receive antenna, y_m, is the sum of the transmitted signals corrupted by the channel and noise, resulting in [2]

$$\begin{aligned} y_m(t) &= \sum_{n=1}^{N_T} \int_{-\infty}^{\infty} h_{mn}(\tau;t) s_n(t-\tau) d\tau \\ &= \sum_{n=1}^{N_T} h_{mn}(\tau;t) * s_n(\tau), \qquad m = 1,2...,N_R \end{aligned} \tag{2.16}$$

where the asterisk implies convolution. The system can therefore be expressed as a system of linear equations as

$$\begin{bmatrix} y_1(t) \\ y_2(t) \\ \vdots \\ y_{N_R}(t) \end{bmatrix} = \begin{bmatrix} h_{11}(\tau;t) & h_{12}(\tau;t) & \cdots & h_{1N_T}(\tau;t) \\ h_{21}(\tau;t) & h_{22}(\tau;t) & \cdots & h_{2N_T}(\tau;t) \\ \vdots & \vdots & \ddots & \vdots \\ h_{N_R 2}(\tau;t) & h_{N_R 2}(\tau;t) & \cdots & h_{N_R N_T}(\tau;t) \end{bmatrix} * \begin{bmatrix} s_1(\tau) \\ s_2(\tau) \\ \vdots \\ s_{N_T}(\tau) \end{bmatrix} \tag{2.17}$$

or more conveniently in matrix form as [2]

$$\mathbf{y}(t) = \mathbf{H}(\tau;t) * \mathbf{s}(\tau) \tag{2.18}$$

where **y** represents the $N_R \times 1$ received matrix and **s** represents the $N_T \times 1$ sent matrix [2].

The result above provides a baseline MIMO channel model. To refine this model we make the following assumptions, taken largely from [2], that will be used throughout this thesis:

1. Thermal noise is present at each receive antenna and is modeled as additive white Gaussian noise (AWGN), denoted as η_m. Further, the AWGN can be characterized as independent identically distributed (IID), each having zero mean and two sided power spectral density $2N_o$.
2. The receiver utilizes a matched filter, whose output is sampled at the end of each symbol interval.
3. The intended receiver has perfect channel estimation. Though this is not practical, it can be very accurately approximated through the use of training symbols.
4. Antenna spacing is sufficient so that the fading on the sub–channels are uncorrelated.

Using these assumptions, the baseline MIMO model can be updated as shown in Figure 4.

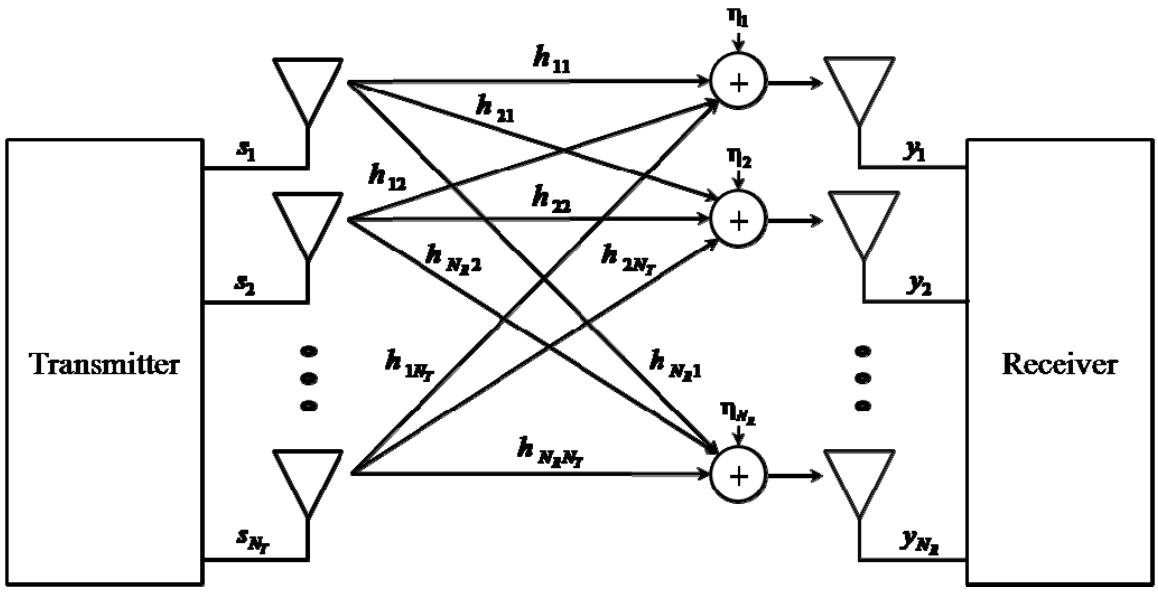

Figure 4. Updated MIMO System Block Diagram (After [2],[3]).

Therefore, $h_{mn}(t)$ can be simplified to h_{mn}, and the composite of the channel coefficients is given by the $N_R \times N_T$ matrix, $\mathbf{H}$ [2]

$$\mathbf{H} = \begin{bmatrix} h_{11} & h_{12} & \cdots & h_{1N_T} \\ h_{21} & h_{22} & \cdots & h_{2N_T} \\ \vdots & \vdots & \vdots & \vdots \\ h_{N_R1} & h_{N_R2} & \cdots & h_{N_RN_T} \end{bmatrix}. \tag{2.19}$$

The $N_R \times 1$ noise matrix, η is given as [2]

$$\eta = \begin{bmatrix} \eta_1 \\ \eta_2 \\ \vdots \\ \eta_{N_R} \end{bmatrix}. \tag{2.20}$$

The received signal, y_m, at each antenna is the sum of the transmitted signals corrupted by the channel and noise, resulting in [2]

$$y_m = \sum_{n=1}^{N_T} s_n h_{mn} + \eta_m, \qquad m = 1, 2..., N_R. \tag{2.21}$$

This can be expressed as a system of linear equations

$$\begin{bmatrix} y_1 \\ y_2 \\ \vdots \\ y_{N_R} \end{bmatrix} = \begin{bmatrix} h_{11} & h_{12} & \cdots & h_{1N_T} \\ h_{21} & h_{22} & \cdots & h_{2N_T} \\ \vdots & \vdots & \vdots & \vdots \\ h_{N_R1} & h_{N_R2} & \cdots & h_{N_RN_T} \end{bmatrix} \begin{bmatrix} s_1 \\ s_2 \\ \vdots \\ s_{N_T} \end{bmatrix} + \begin{bmatrix} \eta_1 \\ \eta_2 \\ \vdots \\ \eta_{N_R} \end{bmatrix} \tag{2.22}$$

or, more conveniently, in matrix form as [2]

$$\mathbf{y} = \mathbf{H}\mathbf{s} + \boldsymbol{\eta} . \tag{2.23}$$

This result will be used throughout the thesis.

C. MULTIPATH CHANNEL MODELS

Over a wireless channel, a radio frequency (RF) signal can take numerous paths to its destination. This is due to objects in the propagation path reflecting, diffracting, and scattering the radio frequency signal as it travels from the transmit antenna to the receive antenna. These paths result in multiple copies of the transmitted signal arriving at the receiver that vary randomly in amplitude, phase and time. Collectively, this is called multipath [5], [7].

Variations in amplitude can produce signals that are too weak to be detected. Differences in phase produce signals that constructively and destructively interfere. Additionally, deviation in arrival time often results in intersymbol interference. That is, symbols which overlap each other in time. In the frequency domain, relative motion of the transmitter, receiver, or the objects between them results in a Doppler shift proportional to the relative velocity of the objects. The significance of these effects are a function of the transmitted signal and either the coherence time $\left(T_C\right)$ or bandwidth $\left(B_C\right)$. That is, how quickly the channel changes in time and frequency respectively. This allows the effects of the fading channel to be classified by four types: slow fading, fast fading, flat fading, and frequency selective fading. This fading classification, relative to the signal bandwidth (B_S) and symbol time (T_S), is depicted in Table 1. [2], [5], [7].

The coherence time of the channel, T_C depends on the Doppler spread, B_D according to the relationship [6]

$$T_C = \frac{1}{4B_D} \tag{2.24}$$

where the Doppler spread is a measure of the spectral expansion due to the relative motion between the transmitter and receiver. If the coherence time is short relative to the symbol duration, then the channel impulse response changes rapidly over the symbol period, causing distortion. The channel is said to be fast fading. On the other hand, if the coherence time is large relative to the symbol period then the channel can be considered static over multiple symbols. The channel is said to be slow fading. Thus, classification of a channel as either fast or slow fading is determined by how quickly the channel is changing in time and the baseband signaling utilized [5]–[7].

The coherence bandwidth of the channel, B_C depends on the multipath delay spread, T_D by the relationship [6]

$$B_C = \frac{1}{T_D} \tag{2.25}$$

where the multipath delay spread is a measure of the difference of arrival times between the longest and shortest propagation paths. Only paths with significant energy are considered. If propagation delay is large (i.e., large T_D) with respect to the symbol duration, then multiple symbols overlap each other at the receiver, causing distortion. The channel is said to be frequency selective. Conversely, if the propagation delay is small compared to the symbol duration, then each path that the symbol takes arrives at the receiver before the next symbol. The channel is said to be frequency non-selective or flat faded. Classification of the channel as either frequency selective or flat faded is determined by how quickly the channel is changing in frequency and the baseband signaling utilized [5]–[7].

Table 1. Characteristics of channel fading (After [6],[7]).

Fast Fading	$B_S < B_D$ $T_s > T_C$
Slow Fading	$B_S > B_D$ $T_s < T_C$

Frequency Selective Fading	$B_S > B_C$ $T_D > T_s$
Frequency Non-Selective Fading (Flat)	$B_S < B_C$ $T_D < T_s$

Therefore, a channel can be characterized and is often referred to by these metrics. This thesis will focus on two statistical models that can be used to represent a frequency non-selective multipath channel: Rayleigh fading and Rician fading. Additionally, the channel is considered slowly fading and the complex channel gain is constant over consecutive symbols.

1. Rayleigh Fading Model

When the communicating antennas do not have a direct line of sight (NLOS) to each other, the received envelope can be modeled as a Rayleigh random process and is referred to as Rayleigh fading. In order to model Rayleigh fading, we utilize the sum of two IID Gaussian random variables with zero mean.

Let Z_{NLOS} represent the sum of two IID Gaussian random variables with zero mean and equal variance

$$Z_{NLOS} = X + jY \tag{2.26}$$

where $X \sim N\left(0, \sigma^2\right)$, $Y \sim N\left(0, \sigma^2\right)$ and the magnitude R is given by

$$R_{NLOS} = \sqrt{X^2 + Y^2}\ . \tag{2.27}$$

In order to relate Equation (2.27) to a distribution, we introduce the joint cumulative distribution function (CDF), defined as [9]

$$F_{X_1X_2}\left(x_1, x_2\right) \equiv \Pr\left[X_1 \le x_1, X_2 \le x_2\right] \tag{2.28}$$

where the CDF is related to the joint probability density function (PDF) by [9]

$$f_{X_1X_2}\left(x_1, x_2\right) = \frac{\partial^2 F_{X_1X_2}\left(x_1, x_2\right)}{\partial x_1 \partial x_2} \tag{2.29}$$

.

Solving for the CDF yields [9]

$$F_{X_1X_2}\left(x_1, x_2\right) = \int_{-\infty}^{x_1}\int_{-\infty}^{x_2} f_{X_1X_2}\left(x_1, x_2\right) dx_1 dx_2 \tag{2.30}$$

thus, expressing Equation (2.27) in terms of the CDF results in

$$F_R\left(r\right) = \iint_{\sqrt{X^2+Y^2}\le r} f_{XY}\left(x, y\right) dxdy \tag{2.31}$$

For $r \ge 0$. Since X and Y are Gaussian random variables, we may further refine Equation (2.31) as

$$F_R\left(r\right) = \left(\frac{1}{\sqrt{2\pi\sigma^2}}\right)^2 \iint_{\sqrt{X^2+Y^2}\le r} e^{\frac{-x^2}{2\sigma^2}} e^{\frac{-y^2}{2\sigma^2}} dxdy \tag{2.32}$$

.

Simplifying Equation (2.32) and performing a change of variables results in

$$F_R\left(r\right) = \left(1 - e^{\frac{-r^2}{2\sigma^2}}\right) u\left(r\right) \tag{2.33}$$

where the unit step function u is given by

$$u\left(r\right) = \begin{cases} 1 & r \ge 0 \\ 0 & r < 0 \end{cases} \tag{2.34}$$

.

Finally, given Equation (2.33), solving for the PDF yields

$$f_R\left(r\right) = \frac{r}{\sigma^2} e^{\frac{-r^2}{2\sigma^2}} u\left(r\right) \tag{2.35}$$

which is the PDF of a Rayleigh distribution. Thus, the sum of two IID complex Gaussian random variables with zero mean as given by Equation (2.26), accurately model Rayleigh fading and provide the desired channel model when NLOS components are present at the receiver [2].

2. Rician Fading Model

For channels with a line of sight (LOS) path in addition to NLOS, the Rician model is more appropriate. However, due to the LOS path, the Gaussian random variables no longer can be modeled with equal mean.

The Rician model follows a Rician distribution given by [7]

$$f_R(r) = \frac{r}{\sigma^2} e^{\frac{-\left(r^2+A^2\right)}{2\sigma^2}} I_0\left(\frac{Ar}{\sigma^2}\right) u(r) \tag{2.36}$$

where $A \geq 0$ and $I_0(\cdot)$ represents the modified Bessel function of the first kind and zero order [7].

Alternatively, this distribution can be described in terms of the *K*–factor, which is defined as the ratio of the energy in the specular (LOS path) to the energy in the diffuse (NLOS paths), given by [8]

$$K \equiv \frac{A^2}{2\sigma^2}. \tag{2.37}$$

The second moment or average received power is the total power of the specular and diffuse paths, given by

$$P_r = A^2 + 2\sigma^2. \tag{2.38}$$

Solving for A^2 and $2\sigma^2$ and substituting Equation (2.37) results in

$$\begin{aligned} A^2 &= \frac{KP_r}{K+1} \\ 2\sigma^2 &= \frac{P_r}{K+1}. \end{aligned} \tag{2.39}$$

Now, the *K*–factor can be used to represent a complex random variable whose magnitude is a Rician random variable, given in Equation (2.36), by utilizing Equation (2.39) as [8]

$$\sqrt{\frac{K}{K+1}}\sigma e^{j\theta}+\sqrt{\frac{1}{K+1}}CN\left(0,\sigma^2\right) \tag{2.40}$$

where the first term is from the specular path and the second term is from the diffuse path. The diffuse path is equivalent to Rayleigh fading described in the previous section.

Thus, by Equation (2.40), Rician fading can be modeled by the sum of a LOS path with uniform phase and NLOS paths as characterized by Equation (2.26) scaled by the *K*–factor. It is easily seen that if $K=0$, Equation (2.40) reduces to a zero mean complex Gaussian, which can be used to model the h_{mn}, for complex channel gains. Additionally, as *K* becomes very large, Equation (2.40) becomes deterministic and would be used for the non–faded case [2].

D. ORTHOGONAL FREQUENCY DIVISION MULTIPLEXING

A primary reason for employing MIMO systems is to achieve higher data rates when compared to single antenna systems. However, as the data rate increases, the symbol time decreases relative to the multipath delay spread. As discussed in the previous section, this produces frequency selective fading which leads to intersymbol interference (ISI) and deep fades, severely degrading performance [10],[11].

To mitigate ISI, multicarrier modulation schemes have been developed that divide the large bandwidth signal into *L* smaller subchannels, where the subchannels are characterized by $\frac{B_S}{L} \ll B_C$. That is, the bandwidth of each subchannel is equal to the signal bandwidth (B_S) divided by the number of total subchannels (*L).* Thus, when *L* is selected to be sufficiently large, the bandwidth of each subchannel is less than the coherence bandwidth of the channel and each subchannel experiences flat fading conditions. The subchannels are then transmitted in parallel such that the bandwidth of the subchannels sum to that of the original signal without the effects of ISI. When the

subchannels are separated in frequency and manipulated to be orthogonal to each other, the multicarrier modulation scheme is called orthogonal frequency division multiplexing (OFDM) [3],[10].

Let $s_k(t)$ represent the carrier signal on the k_{th} subcarrier [2]

$$s_k(t) = \cos 2\pi f_k t \tag{2.41}$$

where $k = 0,1,2,\ldots,L-1$ and f_k is the center frequency of the k_{th} subchannel. The subchannels are orthogonal and independent of the phase between subchannels, over a symbol interval T, when the integral of their product over that same interval is zero, given by [2]

$$\int_0^T \cos\left(2\pi f_k t + \phi_k\right)\cos\left(2\pi f_j t + \phi_j\right)dt = 0 \tag{2.42}$$

where ϕ_k and ϕ_j represent the phase of the k_{th} and j_{th} subchannel respectively and are independent of f_k and f_j. Selecting the OFDM subchannel frequency spacing to be $\frac{1}{T}$ and maintaining the subchannel center frequencies to be integer multiples of each other (i.e., $f_{k+1} - f_k = \frac{1}{T}$ $k = 0,2,\ldots,L-2$) results in the peak of each subchannel corresponding to the nulls of adjacent subchannels. Thus, a set of *L* parallel symbols spaced $\frac{1}{T}$ apart produces *L* orthogonal overlapping signals, providing bandwidth efficiency and minimizing the effects of ISI [2].

1. OFDM-MIMO Transmission

A block diagram showing the transmission OFDM-MIMO system with two transmit antennas (N_T = 2) is given in Figure 5. At the input, data is converted from a binary stream into a set of *L* parallel symbols divided between each antenna and modulate, where the output of the modulator is of the form $X[0], X[1],\ldots, X[N-1]$ and

the symbol rate is reduced by a factor of $\frac{1}{L}$ containing b_k bits. Modulation is typically chosen to be consistent across subcarriers. However, it is possible to modulate each subcarrier with a different scheme.

When L is selected to be an integer multiple of two, then an efficient method known as the Inverse Fast Fourier Transform (IFFT) can be used to implement the inverse discrete Fourier transform (IDFT) given by

$$x[l] = \frac{1}{\sqrt{L}} \sum_{k=0}^{L-1} X[k] e^{\frac{j2\pi lk}{L}} \qquad l = 0,1,\ldots,L-1 \tag{2.43}$$

As can be seen from Equation (2.43), the IDFT takes the components of each subcarrier and produces equivalent time domain symbols that have orthogonal properties mentioned previously.

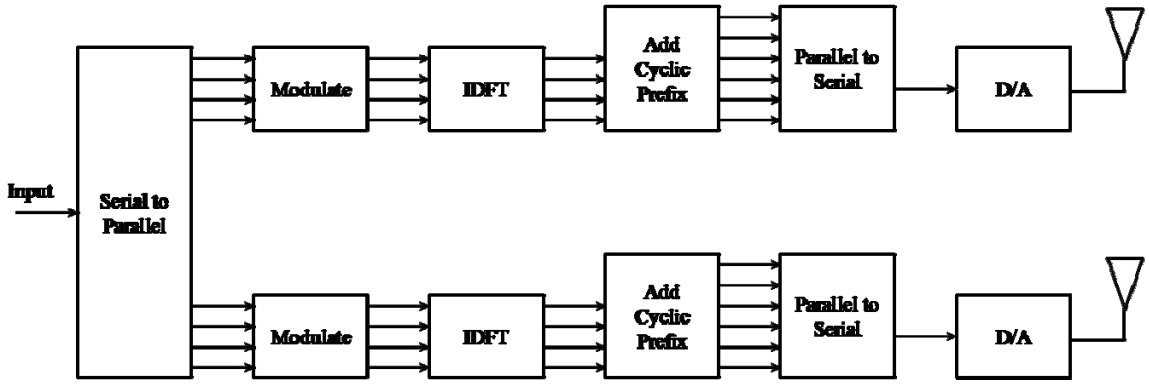

Figure 5. OFDM-MIMO Transmission Block Diagram (After [2]).

The next step in the transmission process is the addition of a cyclic prefix (CP). The CP is created by replicating the data contained in the last part of the symbol and superimposing this copy to the front of the symbol as depicted in Figure 6. The total symbol duration is given by

$$T_{tot} = T_{CP} + T_S \,. \tag{2.44}$$

This is done to guard against the inherent delay of a multipath channel. As introduced in previous sections, as the symbol propagates through the wireless channel, a delay is incurred at the receiver. The cyclic prefix is selected to be of sufficient length as

to prevent the delay of one symbol from corrupting the following symbol. In other words, the cyclic prefix is used as a guard interval to keep the transmitted symbols independent. Obviously, in order to do this, the CP length must be chosen greater than the multipath delay spread of the channel. Another important aspect of the CP and the reason it is appended to the front of a symbol is to protect the start point of the symbol which aids in bit decisions at the demodulator [10].

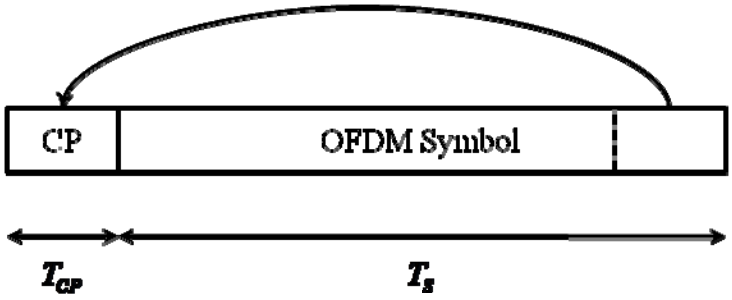

Figure 6. CP of an OFDM Symbol (After [10]).

The symbols are then converted from parallel to a serial sequence, passed through the digital to analog (D/A) converter, and unconverted to radio frequency (RF) for transmission.

2. OFDM Reception

A block diagram showing the OFDM-MIMO system reception process with two receive antennas (N_R = 2) is given in Figure 7. After reception, the signal is down converted and sent through the analog to digital (A/D) converter. The signal is then transformed from a serial sequence into parallel subchannels, where the CP is removed and the discrete Fourier transform (DFT) is implemented with the Fast Fourier Transform (FFT) which is a Fourier pair with the IDFT. Where the DFT is given by

$$X[k] = \sum_{l=0}^{L-1} x[l] e^{\frac{-j2\pi lk}{L}} \tag{2.45}$$

Finally, the subchannels are demodulated and converted back into the binary bit stream.

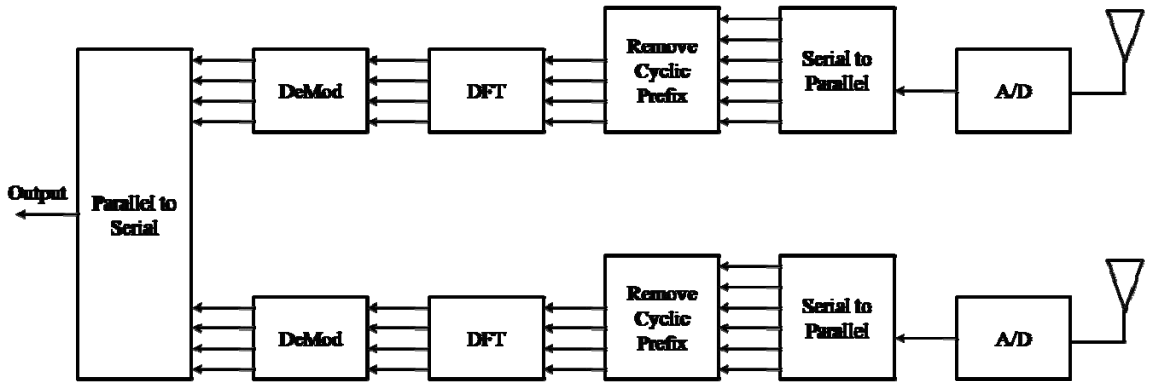

Figure 7. OFDM-MIMO Reception Block Diagram (After [2]).

An OFDM system must maintain synchronization and orthogonality in order to accurately reproduce the original signal. If implemented correctly, the CP will maintain orthogonality by preventing symbol overlap as illustrated by Figure 8. Synchronization can be maintained by allocating OFDM symbols for this purpose. This thesis will assume that the receiver has perfect synchronization and the orthogonality of the symbols is maintained.

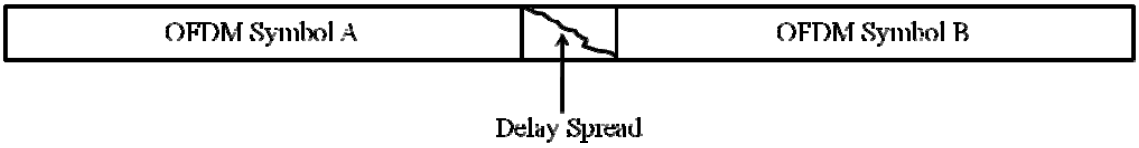

Figure 8. ISI Representation at the Receiver (After [10]).

E. MAXIMUM LIKELIHOOD DETECTION

Recall that the received signal, y_m at each antenna in a MIMO system is the sum of the transmitted signals corrupted by the channel and noise. This was expressed in matrix form by Equation (2.23) and is repeated here, $\mathbf{y} = \mathbf{H}\mathbf{s} + \boldsymbol{\eta}$.

The corruption introduced by the wireless channel requires that the receiver must statistically decide on which symbol was sent based on what was received. To make this decision, the receiver utilizes knowledge of the channel and compares that to the received

signal. For the MIMO model presented in this thesis the optimal method to find this decision statistic is known as Maximum Likelihood (ML) detection. [2]

Bayes' rule forms the basis of the ML detector and is given by [9]

$$\Pr\left[X_1 \mid X_2\right] = \frac{\Pr\left[X_2 \mid X_1\right]\Pr\left[X_1\right]}{\Pr\left[X_2\right]}. \tag{2.46}$$

Let $\Pr\left[X_1\right]$ represent the a priori probability that a particular symbol vector $\mathbf{s}$ was sent, where $\mathbf{s}$ is selected from a known signal space. Let $\Pr\left[X_2\right]$ denote the a priori probability that a particular $N_R \times 1$ decision statistic vector $\mathbf{y}$ was received. Additionally, let $\Pr\left[X_2 \mid X_1\right]$ indicate the a posteriori probability of $\mathbf{y}$ given $\mathbf{s}$ was observed [12].

Observing that sent symbol $\mathbf{s}$ is selected from a finite set of values and the received vector $\mathbf{y}$ is stochastic, Equation (2.46) can be represented more accurately as

$$\Pr\left(\mathbf{s} \mid \mathbf{y}\right) = \frac{f\left(\mathbf{y} \mid \mathbf{s}\right)\Pr\left(\mathbf{s}\right)}{f\left(\mathbf{y}\right)} \tag{2.47}$$

Therefore, the detector needs to select the sent symbol vector that maximizes the probability of the sent symbol vector, given the received vector. Updating Equation (2.47) results in [12]

$$\hat{\mathbf{s}} = \arg\max_{\mathbf{s}} \frac{f\left(\mathbf{y} \mid \mathbf{s}\right)\Pr\left(\mathbf{s}\right)}{f\left(\mathbf{y}\right)} \tag{2.48}$$

where $\hat{\boldsymbol{s}}$ denotes the estimate out of the detector. Assuming that the symbols are sent with equal probability, Equation (2.48) becomes [2]

$$\hat{\mathbf{s}} = \arg\max_{\mathbf{s}} f\left(\mathbf{y} \mid \mathbf{s}\right). \tag{2.49}$$

Since the noise at the receiver is assumed to be IID Gaussian random variables with zero mean, Equation (2.49) can be represented as the minimization of the distance to the stationary vector $\mathbf{y}$, as [13]

$$\hat{\boldsymbol{s}} = \arg\min_{\mathbf{s}} \left|\mathbf{y} - \mathbf{H}\mathbf{s}\right|. \tag{2.50}$$

Thus, the detector compares every possible symbol in the signal space to the received symbol and selects the closest. Alternatively, Equation (2.50) can be expressed in terms of each received symbol [2]

$$\hat{\boldsymbol{s}} = \arg\min_{\mathbf{s}} \sum_{m=1}^{N_R} \left| y_m - \sum_{n=1}^{N_T} h_{mn} s_n \right|^2 . \tag{2.51}$$

F. SPACE TIME CODING

Space-time coding implies multiple antennas either at the transmitter, receiver, or both. They exist to exploit transmit diversity in order to increase channel capacity and reliability. This thesis concentrates on the Alamouti space-time code, introduced in [14].

Figure 9. depicts the scheme when applied to a MIMO system consisting of two transmitters and two receivers. At time t symbols s_1 and s_2 are transmitted simultaneously. At time $t+T$, the negative complex conjugate of s_2 and the complex conjugate of s_1 are transmitted. The result is a sequence of signals shown in Table 2. [14].

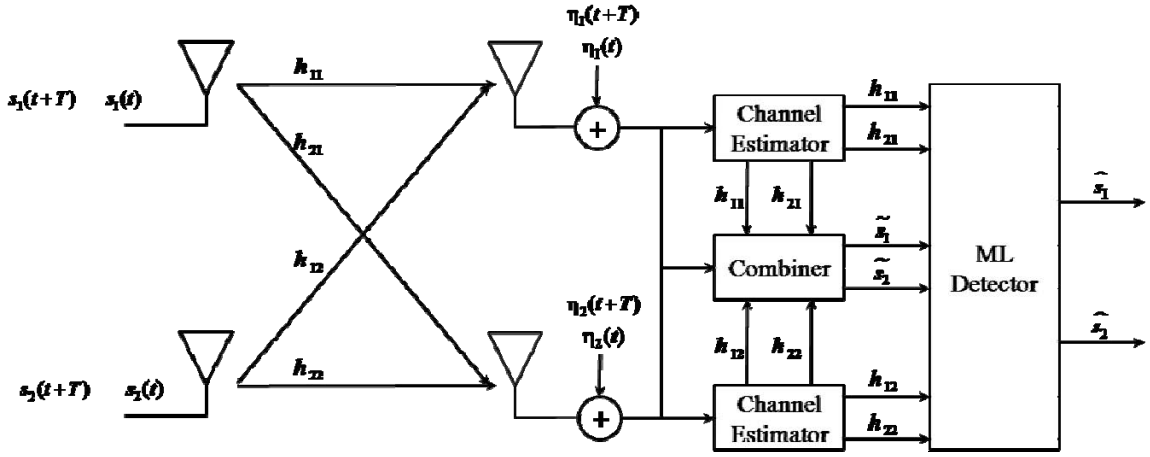

Figure 9. Alamouti Space-Time Coding Scheme (After [14]).

Assuming that the channel remains constant over at least two consecutive symbols, the received signals can then be expressed as [14]

$$
\begin{aligned}
y_1(t) &= h_{11}s_1 + h_{12}s_2 + \eta_1(t) \\
y_2(t) &= h_{21}s_1 + h_{22}s_2 + \eta_2(t) \\
y_1(t+T) &= -h_{11}s_2^* + h_{12}s_1^* + \eta_1(t+T) \\
y_2(t+T) &= -h_{21}s_2^* + h_{22}s_1^* + \eta_2(t+T)
\end{aligned}
\tag{2.52}
$$

where $y_1(t)$ and $y_1(t+T)$ correspond to the received signals at antenna one at time t and $t+T$ respectively. Additionally, $\eta_1(t)$ and $\eta_1(t+T)$ represent the noise components at antenna one at time t and $t+T$ respectively. As mentioned in the previous section, h_{mn} indicates the channel gain to antenna m from antenna n.

Table 2. Alamouti scheme transmission sequence (After [14]).

	Time t	**Time $t+T$**
Transmit Antenna 1	s_1	$-s_2^*$
Transmit Antenna 2	s_2	s_1^*

The received signals are combined and compared. Resulting in symbol estimates given by [14]

$$
\begin{aligned}
\hat{s}_1 &= h_{11}^* y_1(t) + h_{12} y_1(t+T)^* + h_{21}^* y_2(t) + h_{22} y_2(t+T)^* \\
\hat{s}_2 &= h_{12}^* y_1(t) - h_{11} y_1(t+T)^* + h_{22}^* y_2(t) - h_{21} y_2(t+T)^*
\end{aligned}
\tag{2.53}
$$

Substituting Equation (2.52) into Equation (2.53), yields

$$
\begin{aligned}
\hat{s}_1 &= h_{11}^*\left(h_{11}s_1 + h_{12}s_2 + \eta_1(t)\right) + h_{12}\left(-h_{11}^* s_2 + h_{12}^* s_1 + \eta_1(t+T)^*\right) \\
&\quad + h_{21}^*\left(h_{21}s_1 + h_{22}s_2 + \eta_2(t)\right) + h_{22}\left(-h_{21}^* s_2 + h_{22}^* s_1 + \eta_2(t+T)^*\right) \\
\hat{s}_2 &= h_{12}^*\left(h_{11}s_1 + h_{12}s_2 + \eta_1(t)\right) - h_{11}\left(-h_{11}^* s_2 + h_{12}^* s_1 + \eta_1(t+T)^*\right) \\
&\quad + h_{22}^*\left(h_{21}s_1 + h_{22}s_2 + \eta_2(t)\right) - h_{21}\left(-h_{21}^* s_2 + h_{22}^* s_1 + \eta_2(t+T)^*\right)
\end{aligned}
\tag{2.54}
$$

simplifying

$$\begin{aligned}\hat{s}_1 &= \left(|h_{11}|^2 + |h_{12}|^2 + |h_{21}|^2 + |h_{22}|^2\right) s_1 \\ &\quad + h_{11}^{*}\eta_1(t) + h_{12}\eta_1(t+T)^{*} + h_{21}^{*}\eta_2(t) + h_{22}\eta_2(t+T)^{*} \\ \hat{s}_2 &= \left(|h_{11}|^2 + |h_{12}|^2 + |h_{21}|^2 + |h_{22}|^2\right) s_2 \\ &\quad - h_{11}\eta_1(t+T)^{*} + h_{12}^{*}\eta_1(t) - h_{21}\eta_2(t+T)^{*} + h_{22}^{*}\eta_2(t+T).\end{aligned} \tag{2.55}$$

From Equation (2.55) it is clear that the combined symbols are heavily affected by the channel gains. Therefore, the Alamouti scheme provides transmit diversity such that the effects of multipath fading are minimized. The symbols $\hat{s}_1$ and $\hat{s}_2$ are sent to the maximum likelihood detector, discussed in the previous section, and results in symbol estimates $\hat{s}_1$ and $\hat{s}_2$.

Another benefit of the Alamouti scheme is that it achieves full diversity while maintaining low complexity at the receiver. This is due to the orthogonality of the sequence of signals, shown in Table 2. The coding matrix is given by [14]

$$G = \begin{bmatrix} s_1 & -s_2^{*} \\ s_2 & s_1^{*} \end{bmatrix} \tag{2.56}$$

where G is the Alamouti generator matrix for a 2×2 MIMO system. It can be seen that the row vectors are orthogonal

$$v_1 \cdot v_2^{*} = 0 \tag{2.57}$$

where $v_1 = \begin{bmatrix} s_1 & -s_2^{*} \end{bmatrix}$ and $v_2 = \begin{bmatrix} s_2 & s_1^{*} \end{bmatrix}$. Due to this orthogonality, the maximum likelihood detector no longer needs to compare each possible transmitted symbol to the one received. Thus, the complexity of the ML detector is reduced from M^2 to $2M$ possibilities, where M represents the number of possible received symbols in a given modulation scheme (i.e., M-QAM). It is clear that this will significantly reduce computational time requirements [2].

G. CHANNEL STATE INFORMATION AT THE TRANSMITTER

When the transmitter has access to channel characteristics by means of a feedback loop or another method, it is said to know the channel state. With channel state

information at the transmitter (CSIT), capacity can be increased by allocating more power to antennas with favorable channels [2].

Let the channel gain matrix $\mathbf{H}$ be known to the transmitter and receiver. The singular value decomposition (SVD) of $\mathbf{H}$ is given by

$$\mathbf{H} = \mathbf{U}\Sigma\mathbf{V}^H \tag{2.58}$$

where $\mathbf{U}$ is an $N_R \times N_R$ matrix, $\mathbf{V}$ is a $N_T \times N_T$ matrix and both are unitary, that is $\mathbf{U}^H\mathbf{U} = \mathbf{I}_{N_R}$ and $\mathbf{V}^H\mathbf{V} = \mathbf{I}_{N_T}$. Σ is a $N_R \times N_T$ diagonal matrix of the singular values of the channel, denoted by $\sqrt{\lambda_i}$, where i is determined by the rank of $\mathbf{H}$ denoted by r and given by $r \le \min\left(N_T, N_R\right)$. $\mathbf{A}^H$ denotes the Hermitian operator, $\mathbf{A}^H = \left(\mathbf{A}^*\right)^T$ [4].

Substituting Equation (2.58) into the received signal vector given by Equation (2.23), yields

$$\mathbf{y} = \mathbf{U}\Sigma\mathbf{V}^H\mathbf{s} + \boldsymbol{\eta}. \tag{2.59}$$

Defining linear transformations on the received vector as

$$\tilde{\mathbf{y}} = \mathbf{U}^H\mathbf{y} \tag{2.60}$$

the sent vector as

$$\tilde{\mathbf{s}} = \mathbf{V}^H\mathbf{s} \tag{2.61}$$

and noise vector as

$$\tilde{\boldsymbol{\eta}} = \mathbf{U}^H\boldsymbol{\eta} \tag{2.62}$$

then applying these linear transformations to Equation (2.59), yields

$$\begin{aligned} \tilde{\mathbf{y}} &= \mathbf{U}^H\left(\mathbf{U}\Sigma\mathbf{V}^H\mathbf{s} + \boldsymbol{\eta}\right) \\ &= \mathbf{U}^H\mathbf{U}\Sigma\mathbf{V}^H\mathbf{V}\tilde{\mathbf{s}} + \mathbf{U}^H\boldsymbol{\eta} \\ &= \Sigma\tilde{\mathbf{s}} + \tilde{\boldsymbol{\eta}} \end{aligned} \tag{2.63}$$

where $\tilde{\boldsymbol{\eta}}$ is distributed identically to $\boldsymbol{\eta}$. When the transformation of Equation (2.61) is applied to the channel input s, it is often called transmit precoding. When the transformation of Equation (2.60) is applied to the output y, it is referred to as receiver

shaping. From Equation (2.63), it is clear that the SVD operation allows the channel to be represented by rank, r parallel channels, as is illustrated in Figure 10. [2].

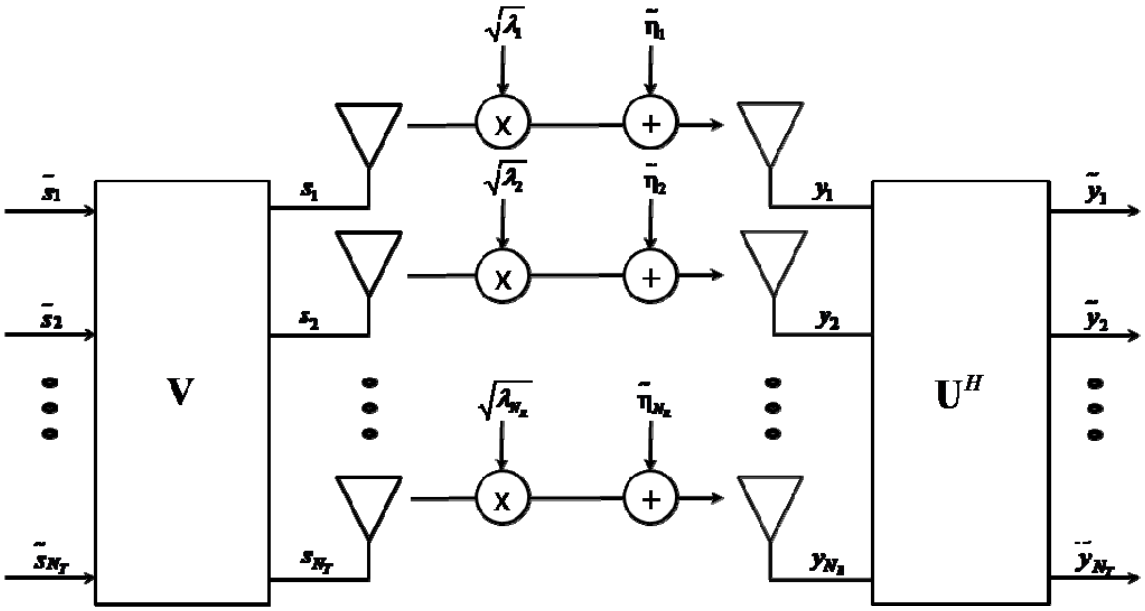

Figure 10. Equivalent MIMO model (After [4]).

This thesis will focus on the ability of the transmitter to reduce errors by allocating power to the individual antennas based on the dominant eigenvalues or singular values of the channel $\sqrt{\lambda_i}$. This process is repeated every symbol period to reduce the probability of errors. If the channel state is unknown, then the power is distributed evenly among all antennas [2],[3].

Given the following total power constraint [4]

$$P = \sum_{i=1}^{N_T} P_i \tag{2.64}$$

where P_i is the power allocated to antenna i and P is the total power. Let the channel capacity be given as [4]

$$C = B\sum_{i=1}^{N_T} \log_2\left(1+\frac{P_i\lambda_i}{\sigma^2}\right) \tag{2.65}$$

where C is the channel capacity, B represents the bandwidth, and σ^2 is the noise power of each element of η. Optimization of the channel capacity in terms of the antenna power allocation is given by [4]

$$P_i = \max\left(\mu - \frac{\sigma^2}{\lambda_i}, 0\right) \tag{2.66}$$

where μ denotes a constant that is adjusted until Equation (2.64) is satisfied. If the channel gain is low, then reliable communication is unlikely and the transmitter allocates less power to that antenna. Iterations are conducted in this manner until the transmitter deems the remaining channels adequate, resulting in optimal power distribution [4],[5].

H. SUMMARY

This chapter introduced the MIMO system model which forms the basis for follow-on analysis. The effects of multipath fading on a wireless channel were introduced and two statistical models defined to aid in analysis. The fundamentals of orthogonal frequency division multiplexing (OFDM) were presented and a MIMO-OFDM system model was introduced utilizing the discrete Fourier transform (DFT). An optimal detection scheme in the form of Maximum likelihood (ML) at the receiver was discussed. Then the Alamouti Space-time coding method for a 2×2 MIMO system was introduced. Finally, channel state information is defined for application at the transmitter where a power allocation process was developed. MIMO systems containing various aspects presented in this chapter are developed and simulated in the following chapter.

THIS PAGE INTENTIONALLY LEFT BLANK

III. ANALYSIS AND SIMULATION

This chapter provides bit error performance analysis and simulation of the two transmit and two receive antenna baseband MIMO model presented in the last chapter. The analysis begins with an uncoded narrowband system and progresses by implementing the various schemes introduced in the previous chapter, culminating with a system utilizing CSIT. To this, a second system is added and analyzed where this second receiver enjoys none of the benefits intended for the primary receiver. Each system was coded and simulated in MATLAB. The source code can be requested from the manager of the Communications Research Laboratory (CRL), at the Naval Postgraduate School.

A. SIMULATION METHODOLOGY AND ASSUMPTIONS

The following assumptions are made when conducting the simulations, which are described in detail in the previous chapter.

Given a fixed wireless communication system comprised of two transmit and two receive antennas, where each antenna is spatially and angularly independent from the other. The information transmitted from each antenna uses the same modulation, either MPSK or MQAM, selected from a signal space as illustrated in Figure 11. The probability of bit error (P_b) for each scheme is inversely related to the distance between closest symbols and is a measure of the number of bits in error per bit sent over a given time interval. Furthermore, the modulation utilizes Gray coding, in that adjacent symbols differ by only one bit. Both signals are transmitted with equal power, split among the two antennas. The total received power from all receive antennas per symbol time is given by [19]

$$\sum_{n} E\left[\left|s_n\right|^2\right] = 1 \tag{3.1}$$

Due to the statistical independence of $\left|s_n\right|$, Equation (3.1) can be expressed for each individual value as

$$E\left[\left|s_n\right|^2\right] = \frac{1}{N_T} \tag{3.2}$$

In the remaining analysis and simulations, for each modulation scheme, E_b is determined and held constant while N_o is adjusted according to the simulated E_b/N_o.

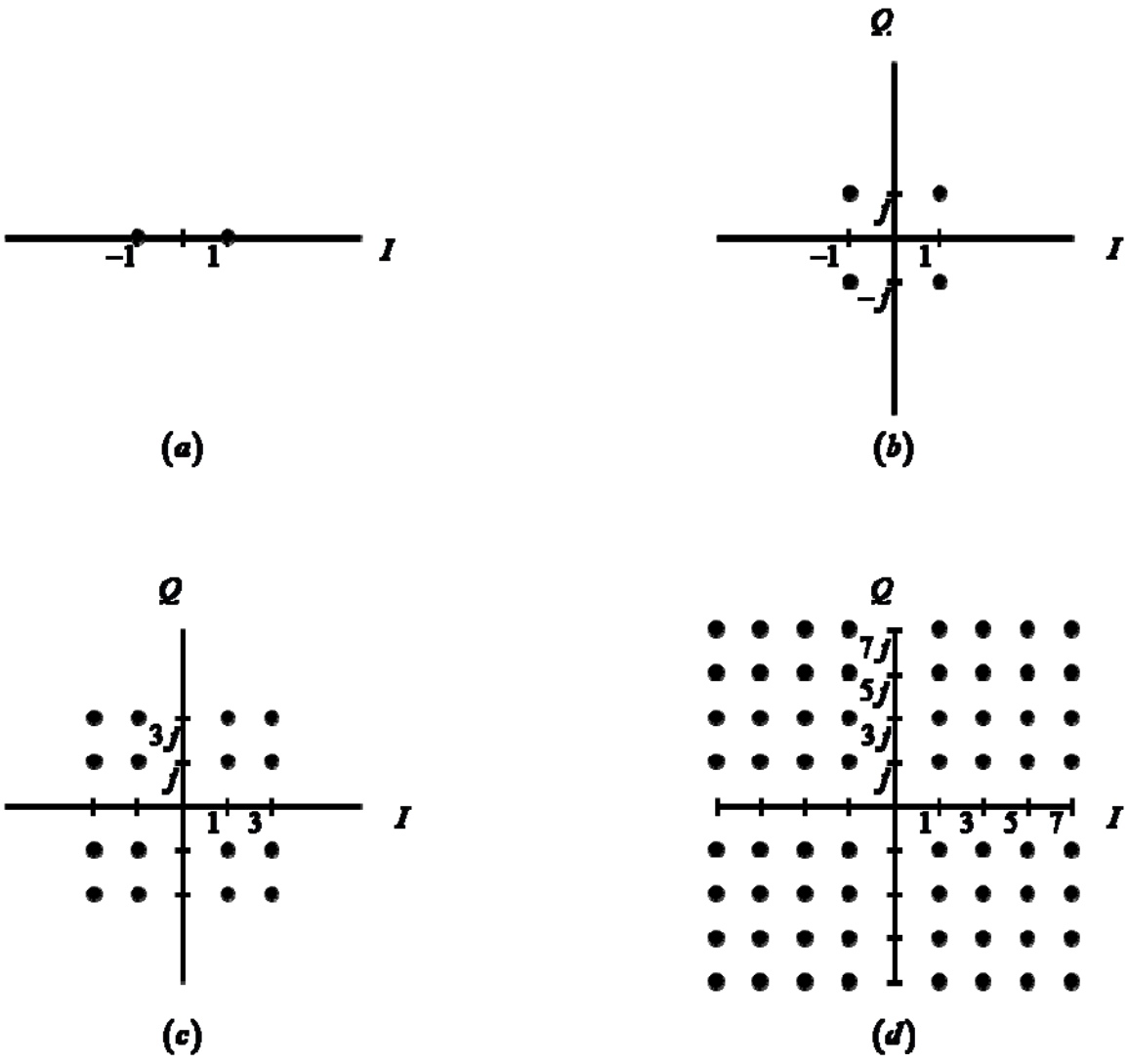

Figure 11. Signal Space for (a) BPSK, (b) QPSK, (c) 16QAM, (d) 64QAM.

The channel is slow frequency non-selective fading and is modeled as having an AWGN, Rayleigh, or Rician distribution. Additionally, the channel gains h_{mn} are

identically distributed and statistically independent from each other and their sum is normalized to unity, given by [2]

$$\sum_{n,m} E\left[\left|h_{mn}\right|^2\right] = 1 \tag{3.3}$$

Due to the statistical independence of h_{mn}, Equation (3.3) can be expressed for each individual value as

$$E\left[\left|h_{mn}\right|^2\right] = \frac{1}{N_T N_R}. \tag{3.4}$$

Thus, the average total energy per bit received is the transmitted energy per bit per transmit antenna. In other words, increasing the number of transmit or receive antennas reduces the channel gains of the system. This may seem counter intuitive, since we would expect that a system employing a greater number of antennas would result in more received power and thus larger energy per bit. However, this assumption is consistent with the literature, namely [2], [3], [5], and will be utilized in this thesis.

Synchronization is maintained perfectly and the channel is known to the receiver, but unknown to the transmitter. The receiver noise is modeled as independent and identically distributed complex white Gaussian noise processes, each having zero mean and power spectral density of $2N_o$. Detection is accomplished by utilizing a maximum-likelihood detector, which provides a best case for probability of error. With the exception of equal power transmission and channel state information at the transmitter, which will be addressed specifically, these assumptions will be used in the proceeding analysis and simulation [2].

B. UNCODED NARROWBAND

The first task is to evaluate the performance of an uncoded MIMO system, as depicted in Figure 12. The entire system is simulated in MATLAB utilizing equivalent baseband form in the discrete time domain. Two million symbols are generated and modulated with either BPSK, QPSK, 16QAM or 64QAM. This is simulated for increasing values of E_b/N_o over the range of 30 dB.

In these simulations, the transmitter employs two antennas with which to transmit the modulated symbols with equal power. The wireless channel is modeled as slowly fading where the signal period is less than the coherence time. The channel gains are simulated according to the AWGN, Rayleigh and Rician models as presented in Chapter II, under the assumptions given in the previous section. At the receiver, a maximum likelihood decision statistic is simulated in which the symbol with the smallest Euclidian distance is selected. This symbol estimate is then demodulated according the appropriate scheme and compared to the transmitted signal. Decision errors are then tallied and calculated over each iteration of E_b/N_o resulting in the following bit error plots.

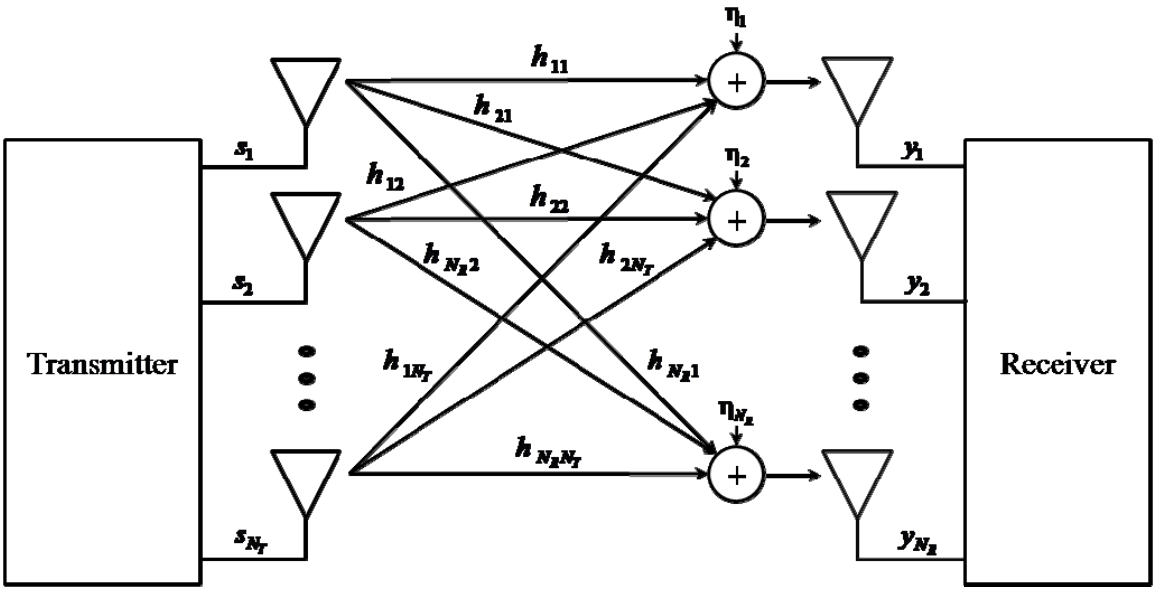

Figure 12. MIMO System Block Diagram (After [2],[3]).

In addition, for comparison and to validate the accuracy of the program, an AWGN channel is simulated and the ideal bit error probability, P_b is presented for each modulation scheme.

In order to compare various modulation schemes of an uncoded 2x2 MIMO system, the average energy per bit is calculated for each modulation scheme with regard to the total energy received during one symbol period.

Let z denote the received signal in the absence of noise, given by

$$z_m = \sum_{n=1}^{N_T} h_{mn} s_n \quad . \tag{3.5}$$

Therefore, the average total energy received over one symbol period is

$$\overline{E_T} = \sum_{m=1}^{N_R} E\left[\left| z_m \right|^2 \right] \tag{3.6}$$

where $E[\bullet]$ is the expectation operator and $\left| z_m \right|^2 = z_m z_m^{\,*}$. Expanding Equation (3.6) we have

$$\begin{aligned} \overline{E_T} &= \sum_{m=1}^{N_R} E\left[\sum_{n=1}^{N_T} h_{mn} s_n \left(\sum_{k=1}^{N_T} h_{mk} s_k \right)^* \right] \\ &= \sum_{m=1}^{N_R} \sum_{n=1}^{N_T} \sum_{k=1}^{N_T} E\left[h_{mn} s_n \left(h_{mk} s_k \right)^* \right] \quad . \end{aligned} \tag{3.7}$$

Due to statistical independence, Equation (3.7) can be simplified

$$\begin{aligned} \overline{E_T} &= \sum_{m=1}^{N_R} \sum_{n=1}^{N_T} \sum_{k=1}^{N_T} E\left[h_{mn} s_n \left(h_{mk} s_k \right)^* \right] \\ &= \sum_{m=1}^{N_R} \sum_{n=1}^{N_T} E\left[\left| h_{mn} \right|^2 \right] E\left[\left| s_n \right|^2 \right] \quad . \end{aligned} \tag{3.8}$$

Recall the previously stated assumptions,

$$\begin{aligned} E\left[\left| h_{mn} \right|^2 \right] &= \frac{1}{N_R N_T} \quad . \\ E\left[\left| s_n \right|^2 \right] &= \frac{1}{N_T} \end{aligned} \tag{3.9}$$

Therefore the total energy received during one symbol period for a 2×2 MIMO system is

$$\begin{aligned} \overline{E_T} &= \sum_{m=1}^{N_R} \sum_{n=1}^{N_T} E\left[\left| h_{mn} \right|^2 \right] E\left[\left| s_n \right|^2 \right] \\ &= \sum_{m=1}^{N_R} \sum_{n=1}^{N_T} \left(\frac{1}{N_T N_R} \right) \left(\frac{1}{N_T} \right) \\ &= \frac{1}{N_T} \end{aligned} \tag{3.10}$$

1. BPSK

The bit error probability for BPSK in a single-input single-output (SISO) AWGN channel is given by

$$P_b = Q\left(\sqrt{\frac{2E_b}{N_0}}\right) \tag{3.11}$$

where E_b denotes the energy per bit and Gaussian Q-function is defined as

$$Q(x) \equiv \int_x^\infty \frac{1}{\sqrt{2\pi}} e^{-y^2/2} dy \tag{3.12}$$

.

Alternatively, the complementary error function is defined as

$$\operatorname{erfc}(x) \equiv \frac{2}{\sqrt{\pi}} \int_x^\infty e^{-t^2} dt \tag{3.13}$$

and is related to the Q-function by

$$Q(x) = \frac{1}{2}\operatorname{erfc}\left(\frac{x}{\sqrt{2}}\right) \tag{3.14}$$

.

Thus, the BER of BPSK in terms of the complementary error function is

$$P_b = \frac{1}{2}\operatorname{erfc}\left(\sqrt{\frac{E_b}{N_0}}\right) \tag{3.15}$$

which is more conducive to programming in MATLAB.

Applying Equation (3.2) to the case of BPSK modulation, where one bit of information is sent every symbol, the energy per bit is given as

$$E_b = \frac{1}{N_T} \tag{3.16}$$

.

Figure 13. shows the performance of BPSK in AWGN, Rayleigh, and Rician channels with $K = 1$ and $K = 4$. The theoretical result obtained via Equation (3.15) is also plotted, which closely follows the simulated AWGN channel.

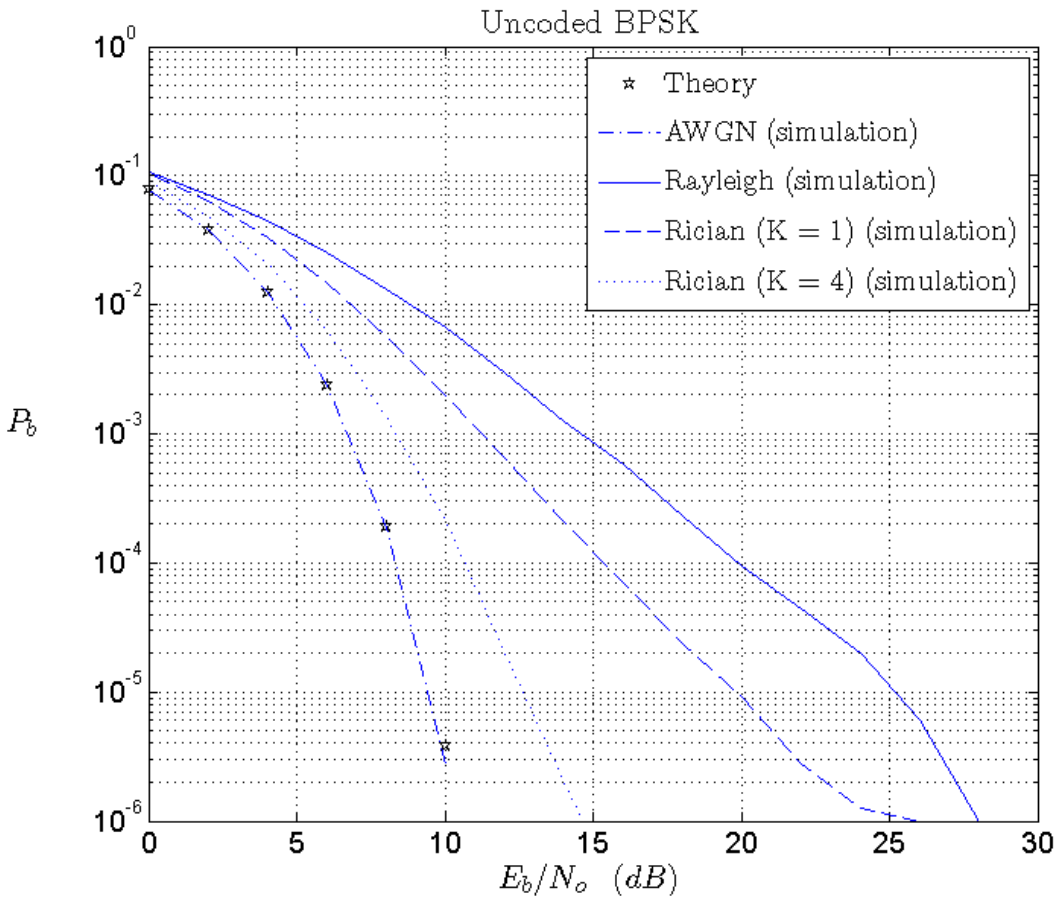

Figure 13. Simulated BER performance of a 2x2 MIMO system with BPSK modulation.

2. QPSK

The bit error probability for QPSK in a SISO AWGN channel is equal to that of BPSK and is given by

$$P_b = Q\left(\sqrt{\frac{2E_b}{N_0}}\right) \tag{3.17}$$

where E_b denotes the energy per bit. Applying Equation (3.2) for QPSK modulation in a 2×2 MIMO system, where two bits of information are sent every symbol, the energy per bit is given as

$$E_b = \frac{1}{2N_T} \tag{3.18}$$

Figure 14. shows the performance of QPSK in AWGN, Rayleigh, and Rician channels with $K = 1$ and $K = 4$. The theoretical result obtained via Equation (3.17) is also plotted. As expected, the results for QPSK match those for BPSK. Therefore, BPSK will not be considered in the remaining analysis.

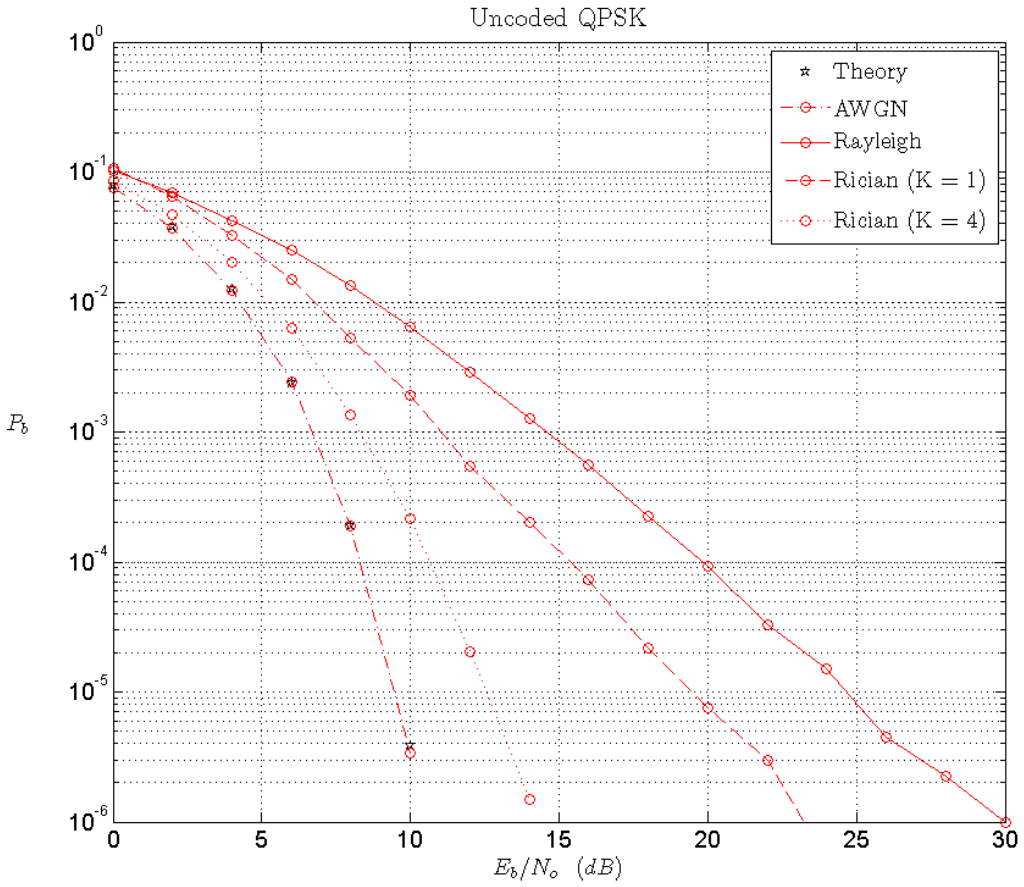

Figure 14. Simulated BER performance of a 2x2 MIMO system with QPSK modulation.

3. 16QAM

Consider a square 16QAM constellation depicted in Figure 11. (c). The symbol error probability for MQAM in an AWGN channel when each symbol selected with equal probability is given by [2]

$$P_s = 4\left(1-\frac{1}{\sqrt{M}}\right)Q\left(\sqrt{\frac{3\log_2 M}{M-1}\left(\frac{E_{b_{avg}}}{N_0}\right)}\right) \tag{3.19}$$

where $E_{b_{ave}}$ denotes the average energy per bit. For the case of 16QAM, Equation (3.19) becomes

$$P_s = 3Q\left(\sqrt{\frac{4}{5}\left(\frac{E_{b_{avg}}}{N_0}\right)}\right) \tag{3.20}$$

By utilizing gray encoding, P_s can be approximated in terms of P_b by [6]

$$P_b \approx \frac{P_s}{\log_2 M}. \tag{3.21}$$

Applying Equation (3.14) and Equation (3.21), the BER of 16QAM in terms of the complementary error function,

$$P_b = \frac{3}{8}\operatorname{erfc}\left(\sqrt{\left(\frac{2}{5}\right)\frac{E_{b_{avg}}}{N_0}}\right) \tag{3.22}$$

The signal space of a square 16QAM constellation is depicted in Figure 11. (c) where the average symbol energy is given by

$$\begin{aligned} E_{s_{avg}} &= \frac{4(2)+8(10)+4(18)}{16} \\ &= 10 \end{aligned} \tag{3.23}$$

when the minimum distance between adjacent vectors is 2 [2]. The relationship between E_b and E_s is

$$E_b = \frac{E_s}{k} \tag{3.24}$$

where k denotes the bits per symbol, $k = \log_2 M$. Thus, the average energy per bit in 16QAM is found to be

$$E_{b_{avg}} = \frac{5}{2}. \tag{3.25}$$

For the case of a 2×2 MIMO system, we have

$$E_b = \frac{5}{2N_T} \tag{3.26}$$

Figure 15. shows the performance of 16QAM in AWGN, Rayleigh, and Rician channels with $K = 1$ and $K = 4$. The theoretical result obtained via Equation (3.22) is also plotted for comparison.

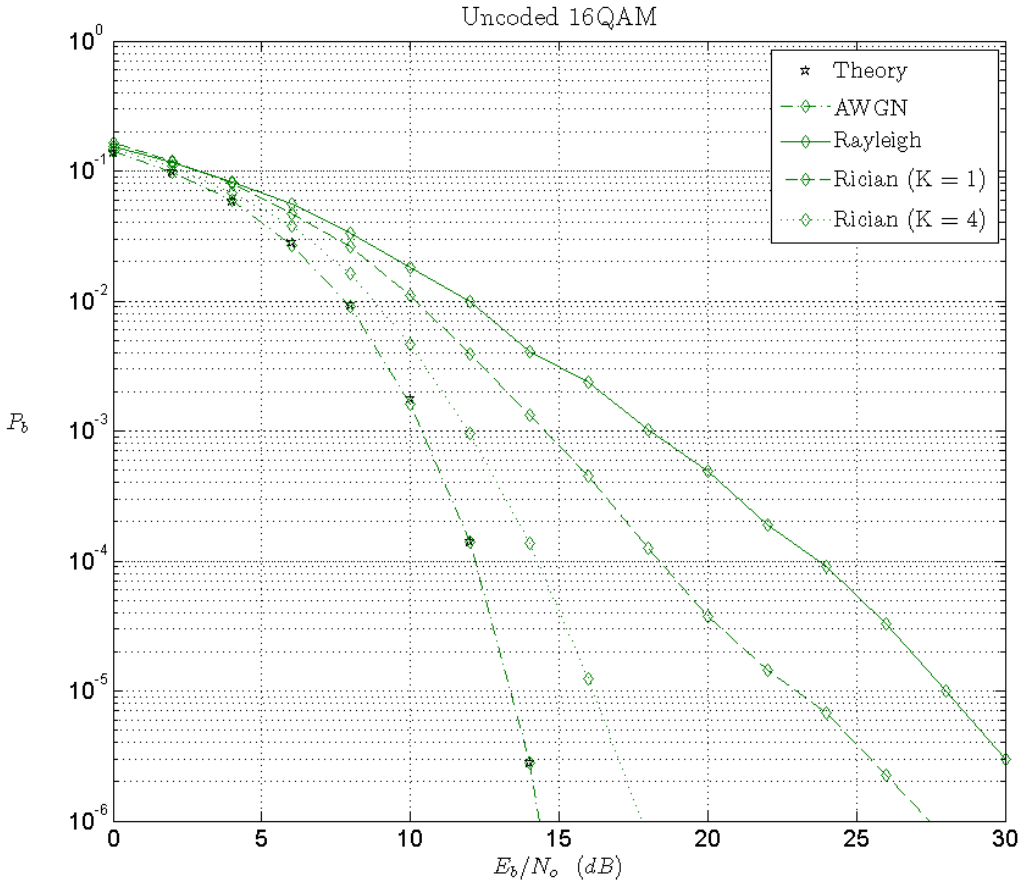

Figure 15. Simulated BER performance of a 2x2 MIMO system with 16QAM modulation.

4. 64QAM

For the square 64QAM constellation depicted in Figure 11. (d), the symbol error probability is given by [2]

$$P_s = \frac{7}{2} Q\left(\sqrt{\frac{2}{7}\left(\frac{E_{b_{avg}}}{N_0} \right)} \right) \tag{3.27}$$

Applying Equation (3.14) and Equation (3.27), the BER of 64QAM in terms of the complementary error function is

$$P_b = \frac{7}{24} \text{erfc}\left(\sqrt{\left(\frac{1}{5} \right) \frac{E_{b_{avg}}}{N_0}} \right) \tag{3.28}$$

and the average symbol energy given by

$$\begin{aligned} E_{s_{avg}} &= \frac{4(2) + 8(10) + 4(18) + 8(26) + 8(34) + 12(50) + 8(58) + 8(74) + 4(98)}{64} \\ &= 42 \end{aligned} \tag{3.29}$$

when the minimum distance between adjacent vectors is 2 [2]. Using Equation (3.24), the average energy per bit of 64QAM modulation is found to be

$$E_{b_{avg}} = 7 \tag{3.30}$$

.

For the case of a 2x2 MIMO system, we have

$$E_b = \frac{7}{N_T} \tag{3.31}$$

Figure 16. shows the performance of 64QAM in AWGN, Rayleigh, and Rician channels. For comparison, the theoretical result obtained via Equation (3.28) is also plotted.

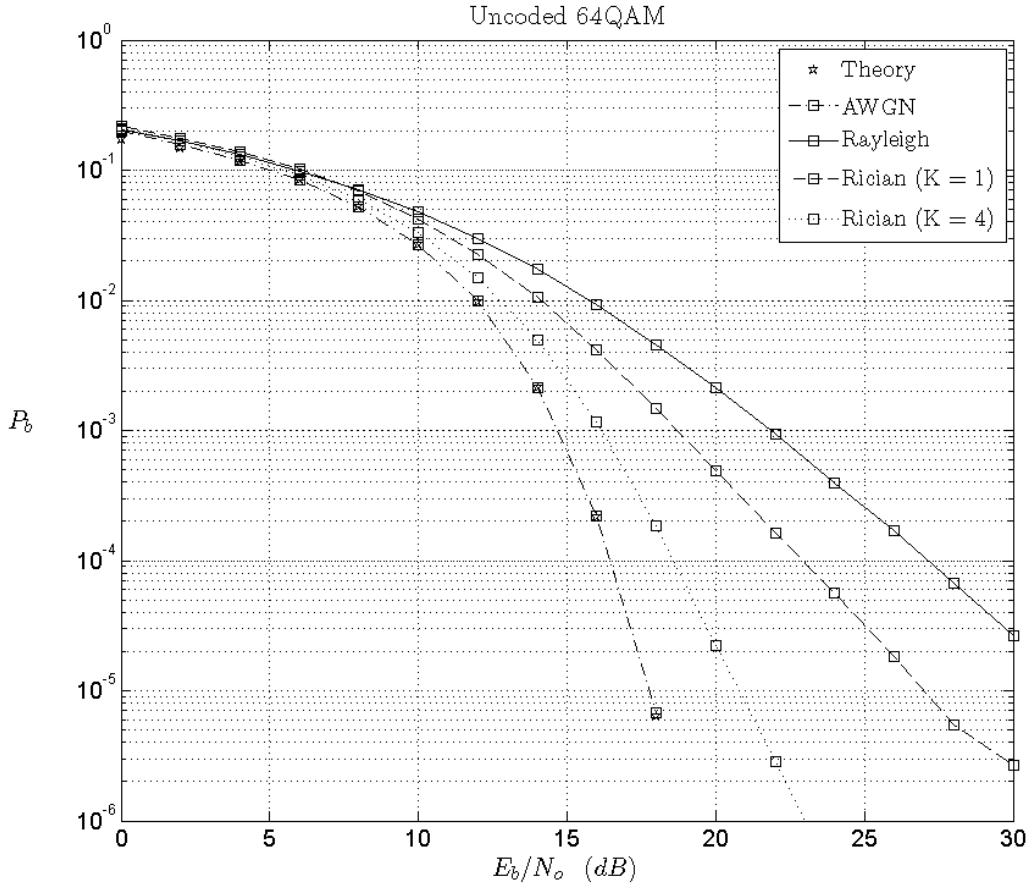

Figure 16. Simulated BER performance of a 2x2 MIMO system with 64QAM modulation.

C. SPACE-TIME CODED NARROWBAND

Building upon the prior section, we evaluate the performance of space time coding with a MIMO system. As before, QPSK, 16QAM and 64QAM modulations are simulated and presented later in this section. The coding implemented follows the Alamouti scheme, introduced in the previous chapter and the following analysis completes that introduction by developing the maximum likelihood decision statistic for equal and non-equal energy constellations.

Figure 17. outlines the system model and the output of the combiner, presented in the previous chapter and reproduced here for convenience.

$$
\begin{aligned}
\tilde{s}_1 &= \left(|h_{11}|^2 + |h_{12}|^2 + |h_{21}|^2 + |h_{22}|^2\right) s_1 \\
&\quad + h_{11}^{*}\eta_1(t) + h_{12}\eta_1(t+T)^{*} + h_{21}^{*}\eta_2(t) + h_{22}\eta_2(t+T)^{*} \\
\tilde{s}_2 &= \left(|h_{11}|^2 + |h_{12}|^2 + |h_{21}|^2 + |h_{22}|^2\right) s_2 \\
&\quad - h_{11}\eta_1(t+T)^{*} + h_{12}^{*}\eta_1(t) - h_{21}\eta_2(t+T)^{*} + h_{22}^{*}\eta_2(t+T)
\end{aligned}
\tag{3.32}
$$

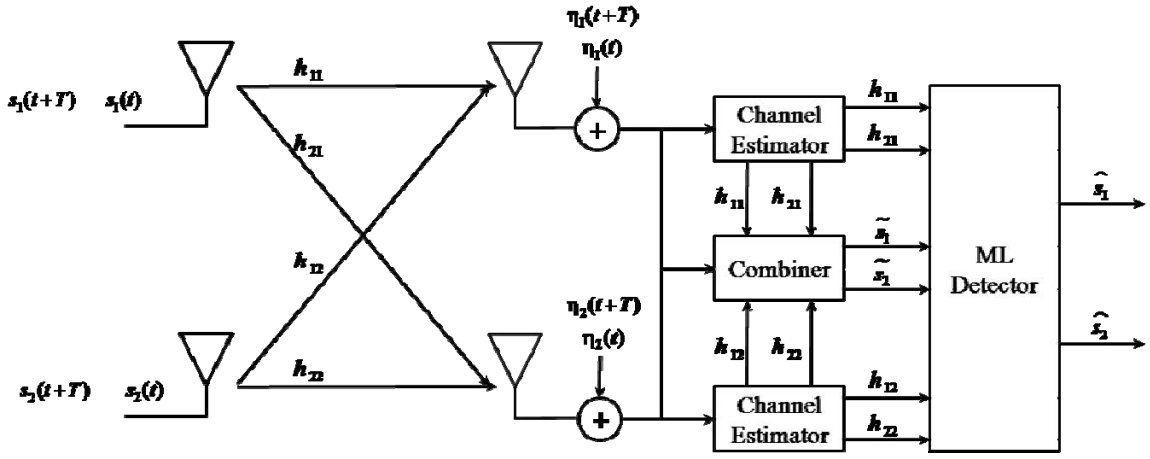

Figure 17. Alamouti space-time coding scheme (After [14]).

The Alamouti scheme uses the following maximum likelihood decision rule to select s_i iff [14]

$$
d^2\left(y_1^1, h_{11}s_i\right) + d^2\left(y_1^2, h_{12}s_i\right) \le d^2\left(y_1^1, h_{11}s_k\right) + d^2\left(y_1^2, h_{12}s_k\right) \tag{3.33}
$$

for all $i \neq k$. The squared Euclidean distance between signals x and y is given by [14]

$$
d^2(x,y) = (x-y)\left(x^{*} - y^{*}\right). \tag{3.34}
$$

Therefore, applying Equations (3.34) and (3.32) to the decision rule gives

$$
\begin{aligned}
&\left(|h_{11}|^2 + |h_{12}|^2 + |h_{21}|^2 + |h_{22}|^2 - 1\right)|s_i|^2 + d^2\left(\tilde{s}_1, s_i\right) \\
&\le \left(|h_{11}|^2 + |h_{12}|^2 + |h_{21}|^2 + |h_{22}|^2 - 1\right)|s_k|^2 + d^2\left(\tilde{s}_1 + s_k\right) \\
&\left(|h_{11}|^2 + |h_{12}|^2 + |h_{21}|^2 + |h_{22}|^2 - 1\right)|s_i|^2 + d^2\left(\tilde{s}_2 + s_i\right) \\
&\le \left(|h_{11}|^2 + |h_{12}|^2 + |h_{21}|^2 + |h_{22}|^2 - 1\right)|s_k|^2 + d^2\left(\tilde{s}_2 + s_k\right)
\end{aligned}
\tag{3.35}
$$

.

Expanding Equation (3.35), the maximum likelihood statistic becomes

$$\min_{s_1}\left[\left(\left|h_{11}\right|^2+\left|h_{12}\right|^2+\left|h_{21}\right|^2+\left|h_{22}\right|^2-1\right)\left|s_i\right|^2-\left(s_i^*\tilde{s}_1+s_i\tilde{s}_1^*\right)\right]$$
$$\min_{s_2}\left[\left(\left|h_{11}\right|^2+\left|h_{12}\right|^2+\left|h_{21}\right|^2+\left|h_{22}\right|^2-1\right)\left|s_k\right|^2-\left(s_i^*\tilde{s}_2+s_i\tilde{s}_2^*\right)\right] \quad (3.36)$$

where the $\left|\tilde{s}_1\right|^2$ and $\left|\tilde{s}_2\right|^2$ terms of the minimum distance calculation are constant and are neglected since they have not impact on the decision. For signals that have equal energy, as in the case of BPSK and QPSK, the magnitudes are constant and the statistic is

$$\min_{s_1}\left[-\left(s_i^*\tilde{s}_1+s_i\tilde{s}_1^*\right)\right]$$
$$\min_{s_2}\left[-\left(s_i^*\tilde{s}_2+s_i\tilde{s}_2^*\right)\right] \quad (3.37)$$

Figure 18. shows the performance of QPSK, 16QAM and 64QAM respectively with space time coding in Rayleigh and Rician channels.

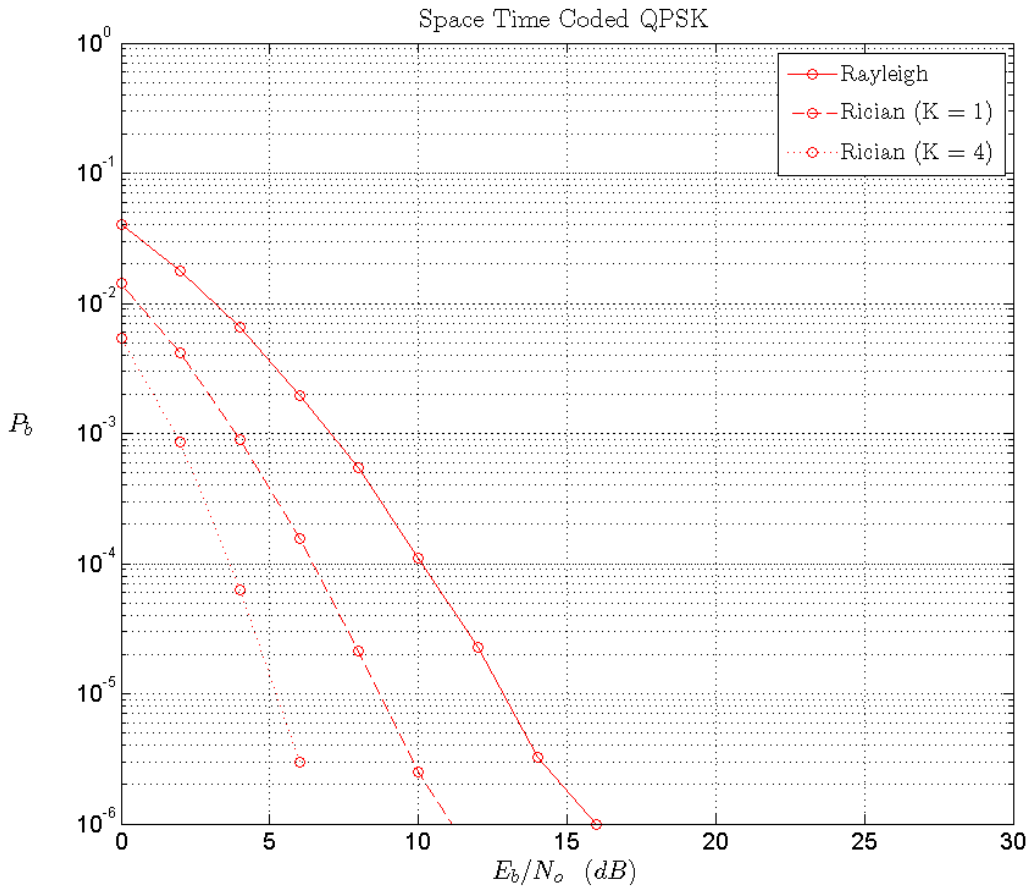

Figure 18. Simulated BER performance of a 2x2 MIMO system with Alamouti space-time coding and QPSK modulation.

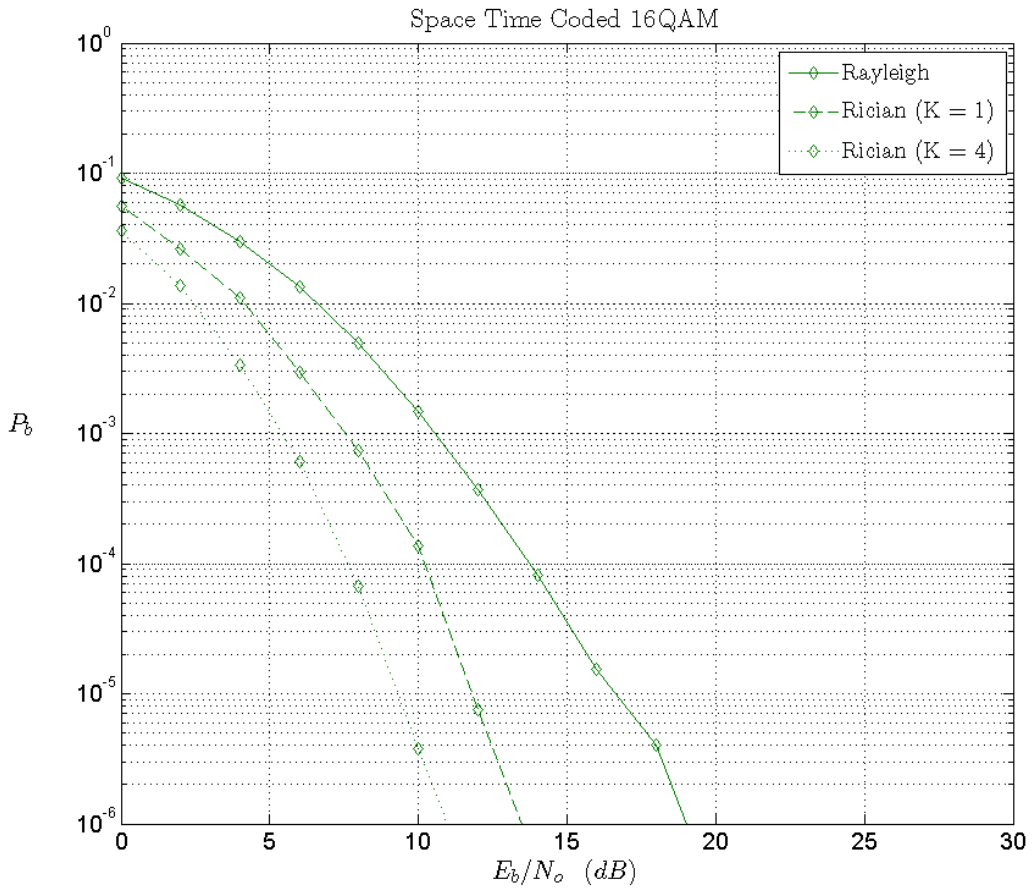

Figure 19. Simulated BER performance of a 2x2 MIMO system with Alamouti space-time coding and 16QAM modulation.

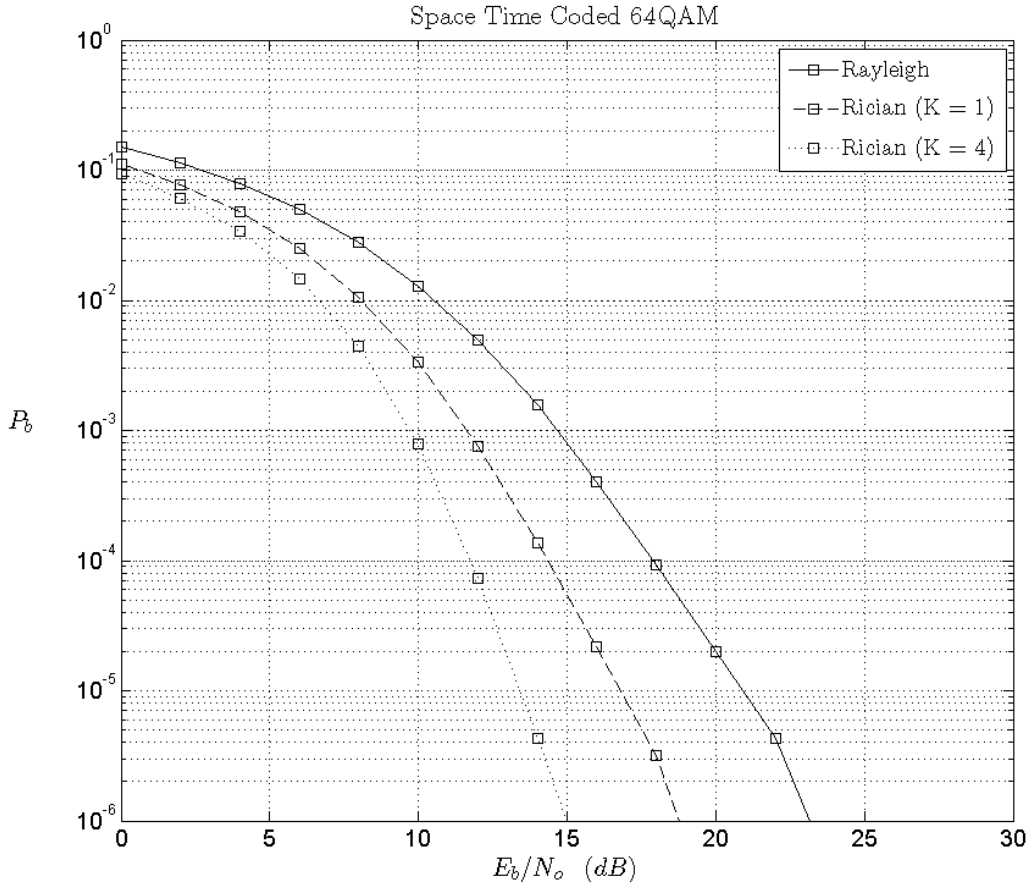

Figure 20. Simulated BER performance of a 2x2 MIMO system with Alamouti space-time coding and 64QAM modulation.

D. SPACE-TIME CODED ORTHOGONAL FREQUENCY DIVISION MULTIPLEXING

We now apply space-time coding to MIMO-OFDM. As a transmission strategy, MIMO and OFDM are integral to 4th generation communications standards. Thus, the bit error performance of such systems is of great interest. This discussion will focus on the implementation of STC, relative to the OFDM system presented in the previous chapter [1].

Consider the basic space-time coded MIMO-OFDM system as shown in Figure 21. The coding scheme is the same as detailed in the previous section; however, the scheme is implemented in the frequency domain on consecutive tones or subcarriers.

Analogous to the time domain implementation, in the frequency domain it is assumed that the channel remains constant over consecutive tones [10].

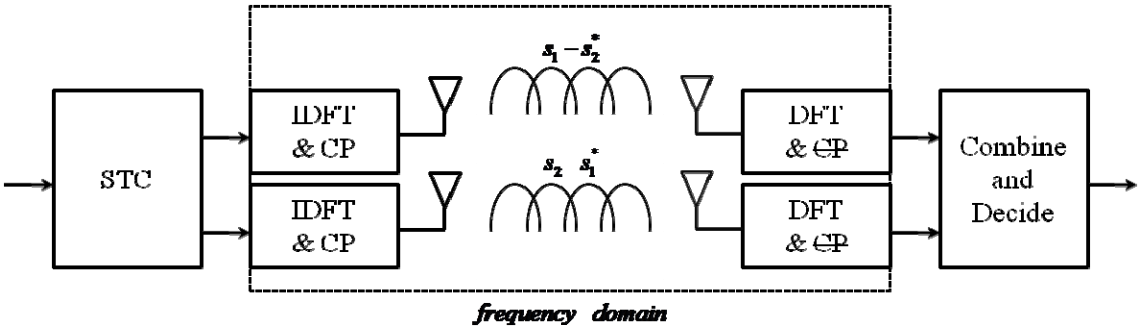

Figure 21. Basic implementation of STC with MIMO-OFDM (After [5]).

The simulation was performed with an FFT size of 512 points and a cyclic prefix of $1/4$. That is, the last 128 points from the output of the IDFT operation were reproduced and appended to the beginning of the symbol in the form of a cyclic prefix. The OFDM symbols are then sent to the transmitter and transmitted through either a Rayleigh or Rician fading channel. At the receiver, the cyclic prefix is removed and the DFT operation is performed. The symbols are then combined and estimated in accordance with the Alamouti scheme where the decision criterion is analogous to the narrowband case presented in the previous section.

The simulation evaluated over two million symbols with E_b/N_o increasing from 0 to 30dB in increments of two dB. The results of QPSK, 16QAM and 64QAM can be seen in Figure 22. Figure 23. and Figure 24. respectively.

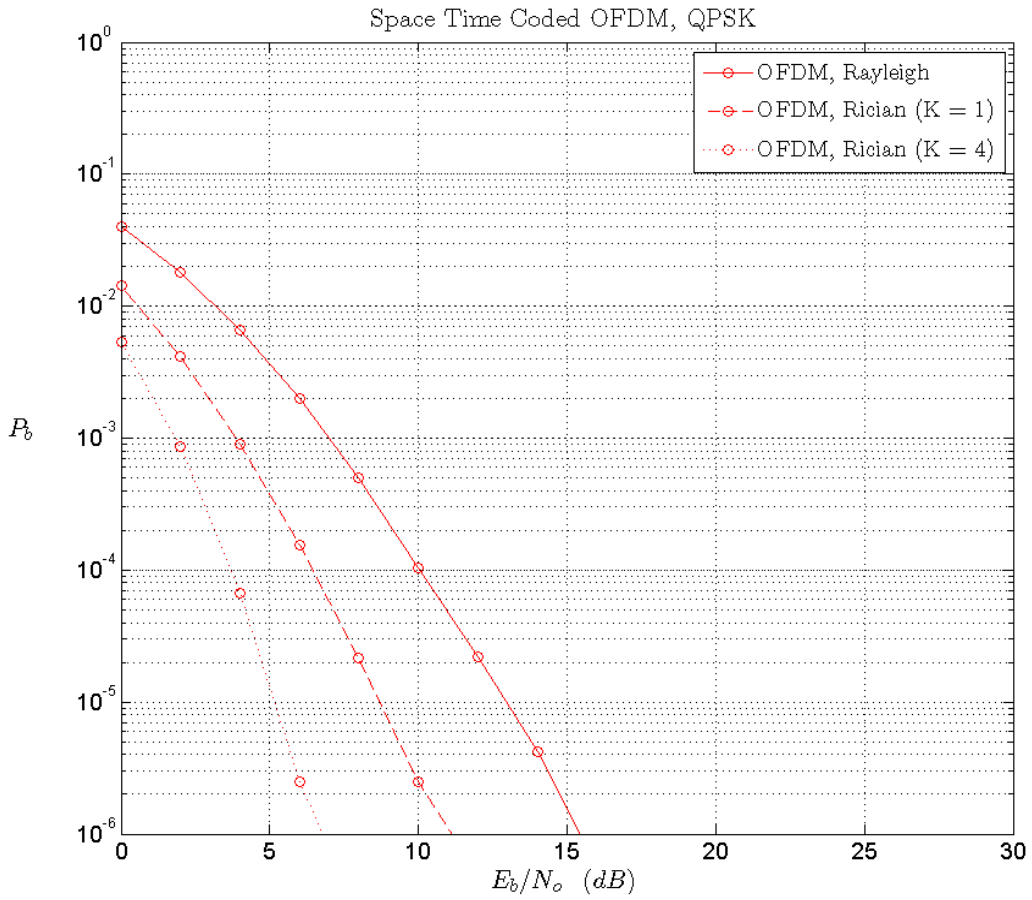

Figure 22. Simulated BER performance of a 2x2 MIMO-OFDM system with Alamouti space-time coding and QPSK modulation.

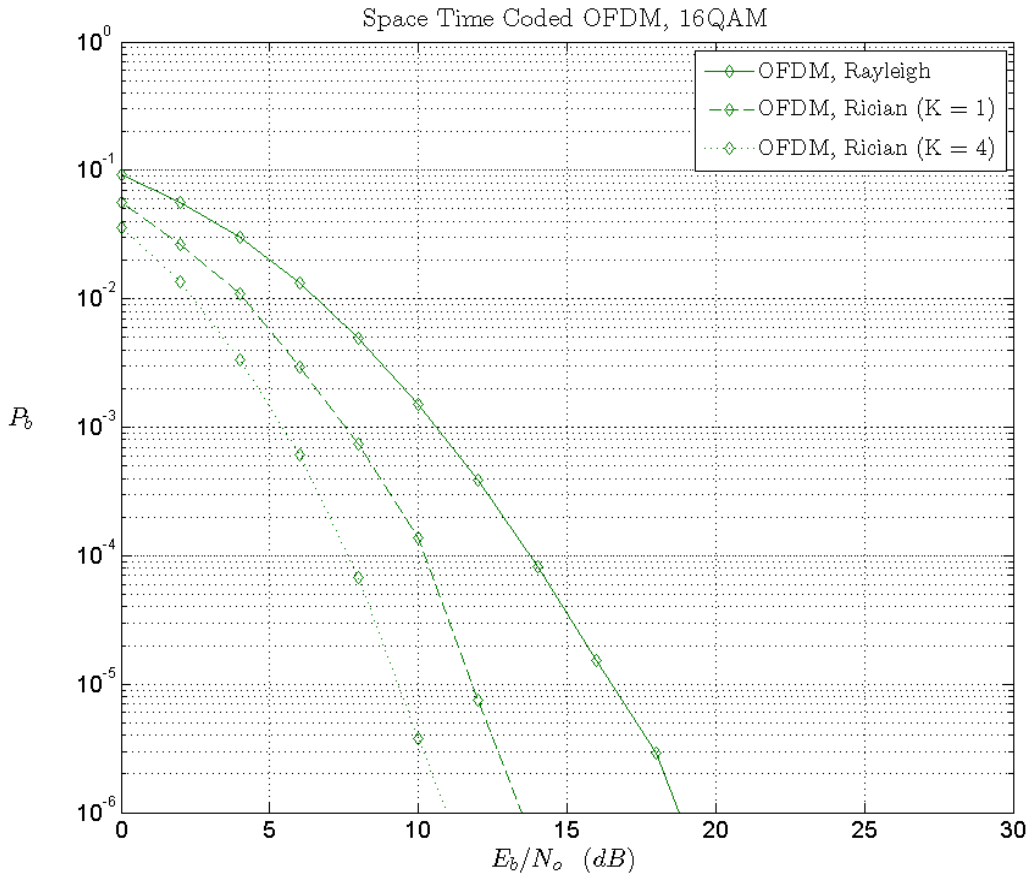

Figure 23. Simulated BER performance of a 2x2 MIMO-OFDM system with Alamouti space-time coding and 16 QAM modulation

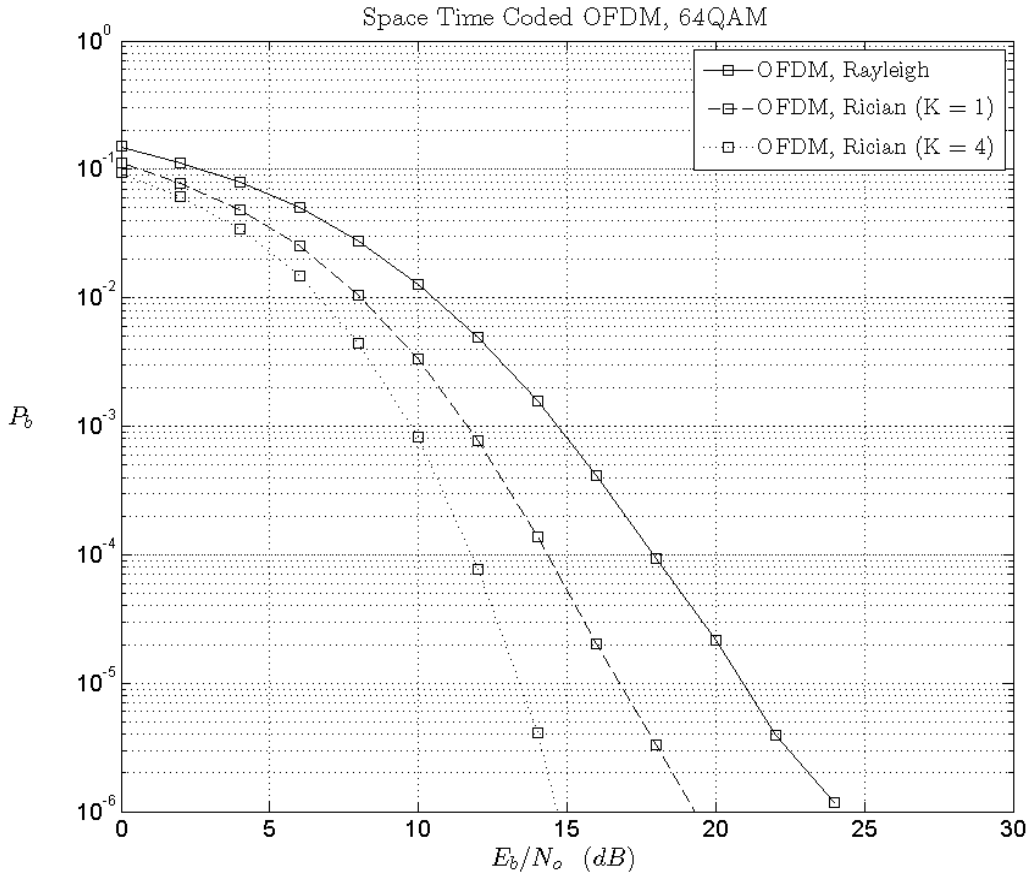

Figure 24. Simulated BER performance of a MIMO-OFDM system with Alamouti space-time coding and 64QAM modulation.

E. NARROWBAND WITH CHANNEL STATE INFORMATION AT THE TRANSMITTER

This section investigates the performance of a 2×2 MIMO system when the channel state is available to the transmitter, often referred to as a closed-loop system. We assume that the antennas are fixed and that the feedback channel provides perfect information on the transmit channel. Figure 25. depicts the basic system. Knowledge of the channel gains allows the transmitter to use various techniques in order to increase capacity or reliability. The following analysis focuses on increasing reliability through diversity techniques. One such method, which requires channel state information at the transmitter, is dominate eigenmode transmission.

Dominate eigenmode transmission is also known as linear diversity precoding, and is analogous to maximal ratio Combining (MRC) in the case of a MISO system. Additionally, dominate eigenmode transmission lends a comparison with the Alamouti scheme of space-time coding, which does not require CSIT. Both techniques provide full diversity order of four, the maximum in the case of a 2×2 system. However, in the case of dominate eigenmode transmission, the channel state information allows the transmitter to optimally precode the signal, which provides an array gain at the receiver not found in the Alamouti scheme.

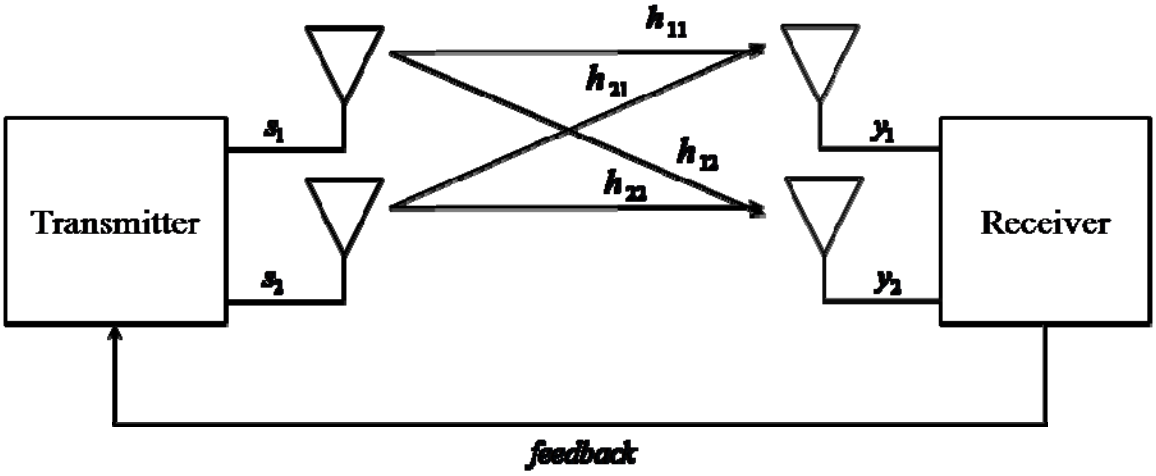

Figure 25. Closed loop model.

Given a 2×2 MIMO system, let the same symbol be transmitted on both antennas during each time period, weighted by a $N_T \times 1$ vector $\mathbf{w}$. Thus, the receiver yields

$$\mathbf{y} = \mathbf{Hws} + \boldsymbol{\eta} \tag{3.38}$$

where $\mathbf{H}$ represents the $N_R \times N_T$ channel matrix, $\boldsymbol{\eta}$ is the $N_R \times 1$ noise vector, $\mathbf{s}$ represents the transmitted symbol and $\mathbf{y}$ is the $N_R \times 1$ received signal vector. At the receiver, the signals are combined and weighted by a $N_R \times 1$ vector $\mathbf{g}$, given by [16]

$$z = \mathbf{g}^H \mathbf{y} \tag{3.39}$$

resulting in

$$\mathbf{z} = \mathbf{g}^H \left(\mathbf{Hws} + \boldsymbol{\eta} \right). \tag{3.40}$$

In order to find the optimal weighting of the transmitted signals, the transmitter utilizes the singular values of the channel. Recall from Chapter II that SVD operation is given as

$$\mathbf{H} = \mathbf{U}\Sigma\mathbf{V}^H \tag{3.41}$$

where $\mathbf{U}$ and $\mathbf{V}$ are $N_T \times N_T$ and $N_R \times N_R$ unitary matrices, and Σ is a $N_R \times N_T$ diagonal matrix of the singular values of the channel. It is shown in [4] that the receiver SNR is maximized when both the postcode vector $\mathbf{g}$, and the precode vector $\mathbf{w}$ correspond to the right and left singular vectors of the maximum singular value of $\mathbf{H}$, $\sigma_{\max}$. Therefore, to maximize the receiver SNR, Equation (3.40) can be represented as

$$\mathbf{y} = \sigma_{\max}\mathbf{s} + \boldsymbol{\eta} \tag{3.42}$$

where $\sigma_{\max}$ is a scalar that corresponds to the largest value in Σ which is the maximum singular value of $\mathbf{H}$. Given that the $\sigma_{\max}$ singular value of $\mathbf{H}$ corresponds to the left and right singular vectors $u_{\max}$ and $v_{\max}$ respectively, we can express Equation (3.42) in terms of the SVD operation by [17]

$$\mathbf{y} = u_{\max}{}^H \mathbf{H} v_{\max}\mathbf{s} + \boldsymbol{\eta} \tag{3.43}$$

The corresponding system model is depicted in Figure 26. Thus, with channel state information, the transmitter weighs the transmitted symbols according to the right singular vector of the channel $\mathbf{H}$. At the receiver, the symbols are summed and weighed by the left singular vector where the signal to noise ratio is given by [3]

$$\gamma = \frac{E_s}{\sigma^2}\sigma_{\max}^2 \tag{3.44}$$

where E_s is the symbol energy, σ^2 is the noise power of each element of $\boldsymbol{\eta}$ and γ is bounded by [4],[9]

$$\frac{E_s \left\| \mathbf{H} \right\|_{\mathbf{F}}^2}{\sigma^2 N_T} \le \gamma \le \frac{E_s \left\| \mathbf{H} \right\|_{\mathbf{F}}^2}{\sigma^2} \tag{3.45}$$

and the Frobenius norm denoted as $\|\square\|_{\mathbf{F}}$ is given by [17]

$$\|\mathbf{H}\|_{\mathbf{F}} = \sqrt{\sum_{i=1}^{N_T}\sum_{j=1}^{N_R} h_{ij}^2} \quad (3.46)$$

Thus, dominant eigenmode transmission provides two types of gain; diversity and array. Since the same symbol is sent from each antenna, the diversity gain is the result of having multiple independent copies of the symbol for decision. At the receiver the optimally weighted and independent signals are coherently combined, providing the array gain. The array gain realized depends on the fading characteristics of the channel and is given by $E\left[\sigma_{\max}^2\right]$ [3][5].

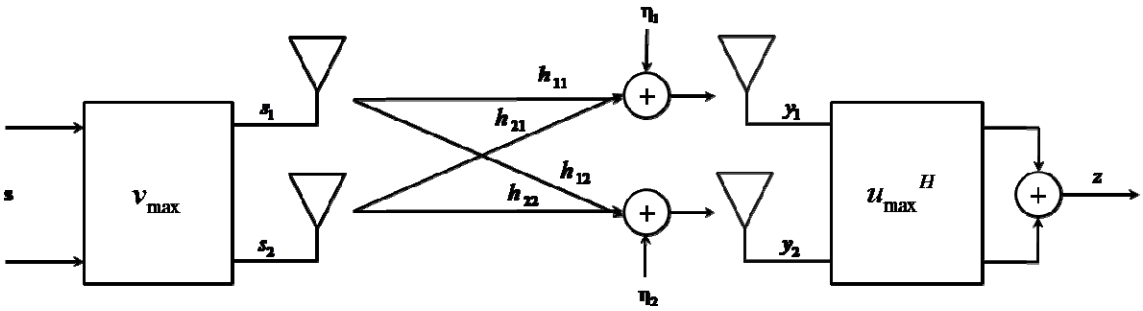

Figure 26. Dominant eigenmode transmission in a 2x2 MIMO system.

Figure 27. provides the performance of QPSK utilizing a dominant eigenmode transmission in Rayleigh and Rician channels.

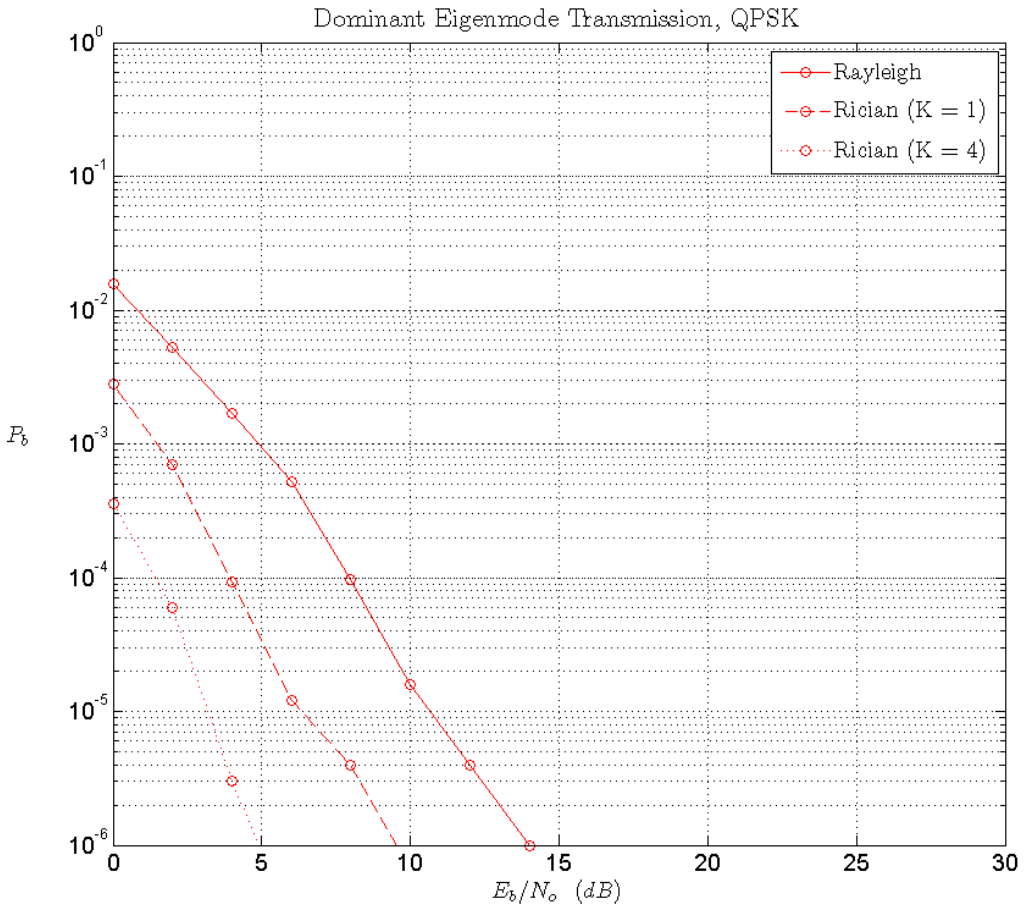

Figure 27. Simulated BER performance of a 2x2 MIMO system with QPSK modulation using dominant eigenmode transmission when the transmitter has channel state information.

F. UNKNOWN RECEIVER

Throughout this chapter, each section presented analysis and performance results of various techniques used in MIMO communications. The implementation of such schemes is often dependant on the environment in which the communication system is operating. Additionally, the many benefits of MIMO communications rely on the successful pairing of the transmitter and receiver, where the result of this pairing is often

the optimization of the transmission link. This is a preferred, indeed desired, outcome for system designers. However, this thesis seeks to investigate how a receiver performs in the absence of this optimization.

Consider a MIMO system containing transmitter A and receiver B as shown in Figure 28. The system is located on fixed infrastructure and has been designed to optimize the link between A and B, a NLOS situation. The transmitter has channel state information, through a feedback loop with receiver B. With CSIT, the transmitter utilizes dominant eigenmode transmission in order to improve the signal to noise ratio at receiver B, providing a robust communications link.

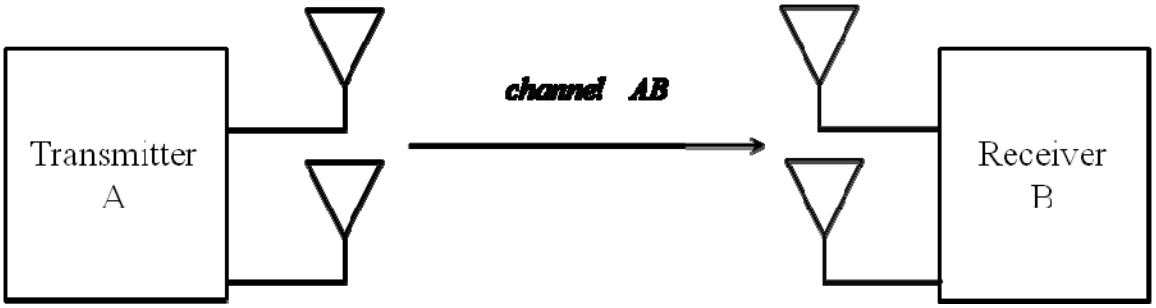

Figure 28. A fixed MIMO system optimized for channel AB.

We now introduce a second receiver, C, that is disadvantaged in the sense that it does not enjoy the same optimization with transmitter A that receiver B has. Receiver C can be mobile or fixed. Channel AC can be either Rayleigh faded channel (NLOS) or a Rician fading channel (LOS). If the receiver is mobile, the velocity is assumed to be such that the assumptions given at the beginning of this chapter still hold. Additionally, the receiver is not limited by the number of antennas available. That is, the receiver may employ additional antennas, greater than two, in order to improve reception. Figure 29. provides the system layout, where the dashed line represents the link that is not optimized.

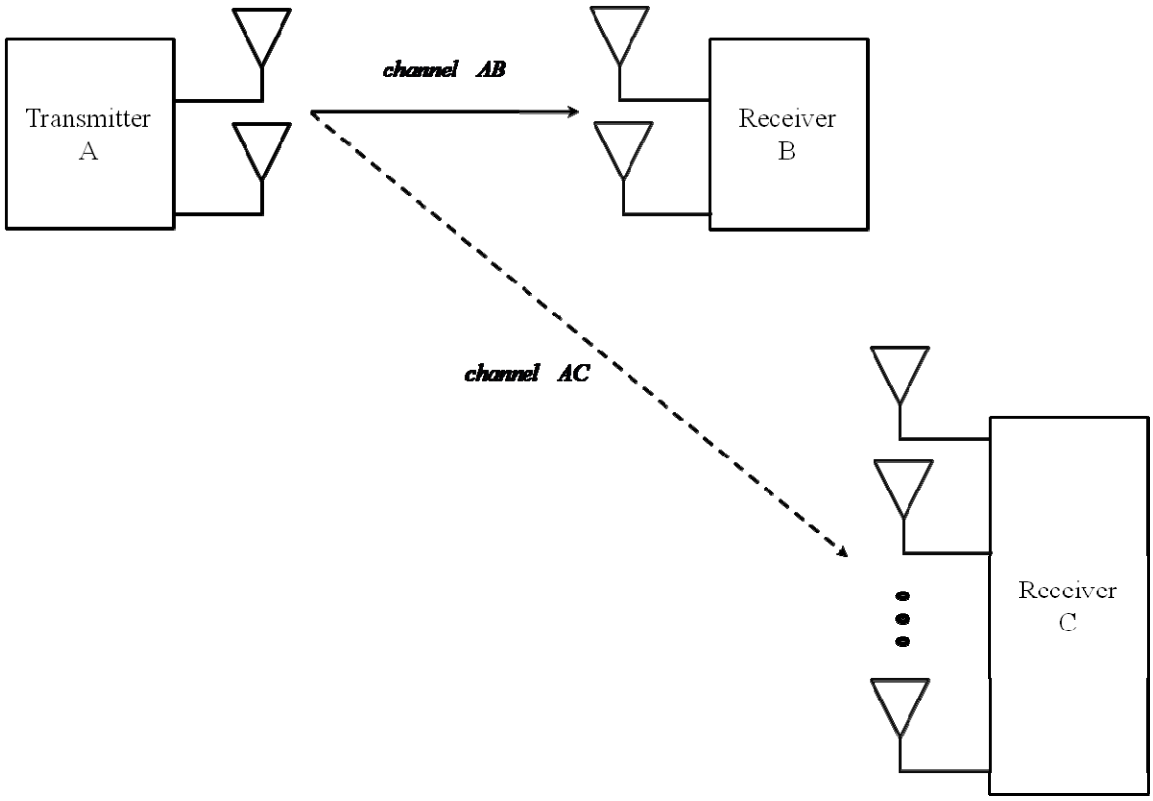

Figure 29. Disadvantaged receiver in a fixed MIMO system optimized for channel AB.

Recall from the previous section that a transmitter with channel state information may precode the transmitted symbols in order to increase the signal to noise ratio at the receiver. This result was shown in Equation (3.42) and is reproduced here for convenience.

$$\mathbf{y} = \sigma_{\max}\mathbf{s} + \boldsymbol{\eta}. \tag{3.47}$$

Expressing Equation (3.47) in terms of the SVD operation we get an equivalent system represented by [17]

$$\mathbf{y} = \left(u_{\max}^{H}\mathbf{H}v_{\max}\mathbf{s} + \boldsymbol{\eta}\right)_{AB} \tag{3.48}$$

where $(\square)_{AB}$ denotes the characteristics of the link from transmitter A to receiver B. We assume that receiver C has knowledge of the precoding vector or the right singular value of the channel $(\mathbf{H})_{AB}$. With this knowledge, the receiver is able to compensate for the optimization induced by the transmitter for channel AB. This case is simulated with

QPSK modulation over four million symbols with E_b/N_o increasing by increments of two dB. Three situations are presented: The first involves a Rayleigh channel, the second involves a Rician channel with rice factor of one $(K=1)$, and the final situation simulates a Rician channel with $(K=4)$. Additionally, all three scenarios are evaluated with receiver C having 2, 4, and 8 antennas. The results are plotted in Figure 30. Figure 31. and Figure 32. ,, respectively.

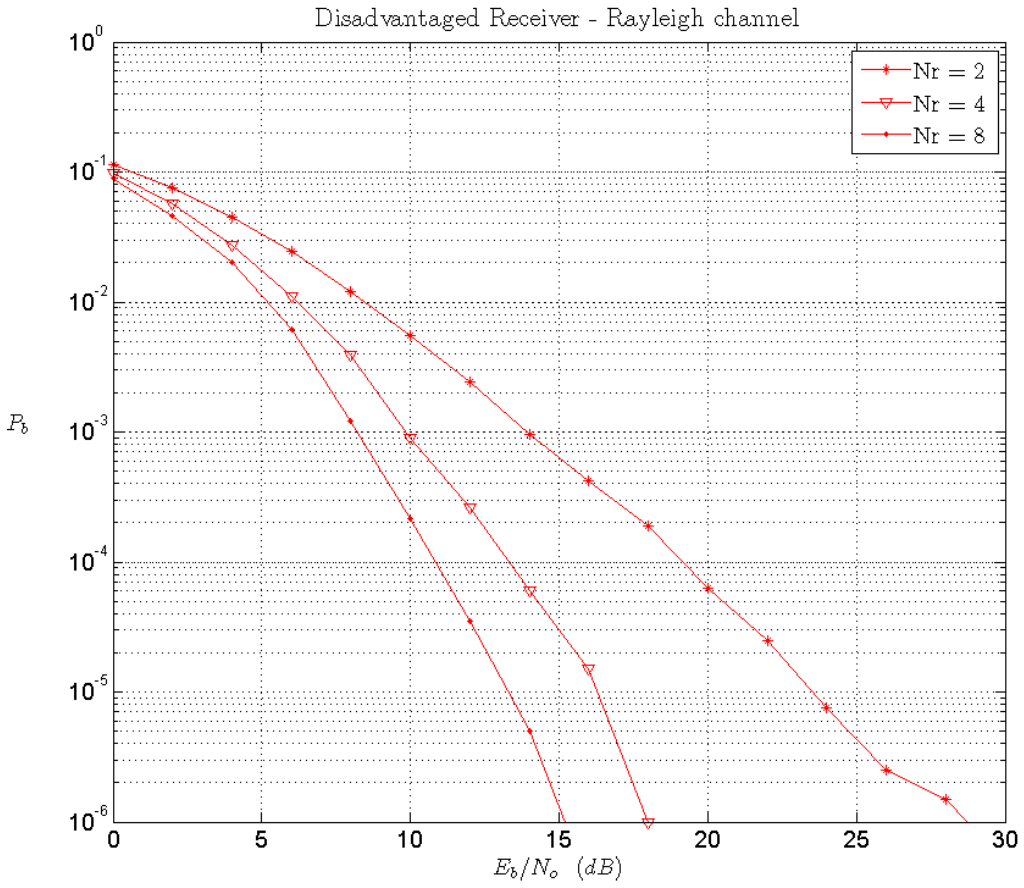

Figure 30. Simulated BER performance of the disadvantaged receiver in a Rayleigh channel, for 2x2, 2x4, and 2x8 MIMO systems.

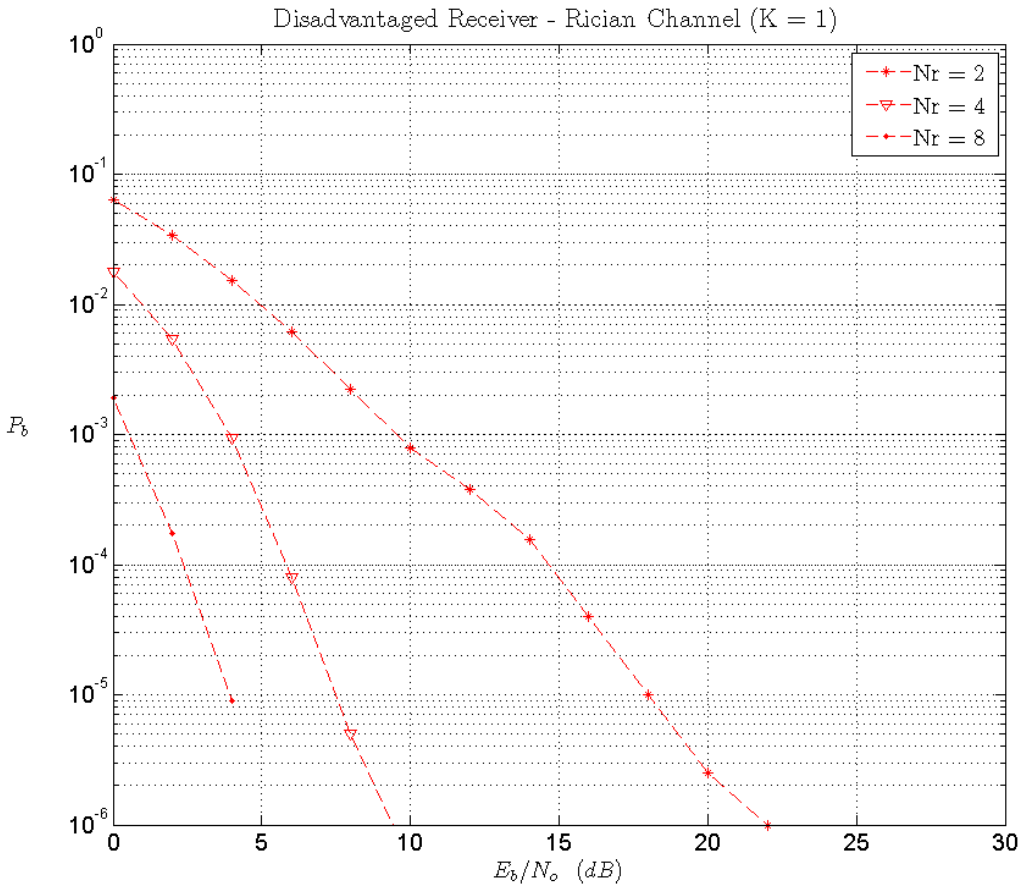

Figure 31. Simulated BER performance of the disadvantaged receiver in a Rician channel (K=1), for 2x2, 2x4 and 2x8 MIMO systems.

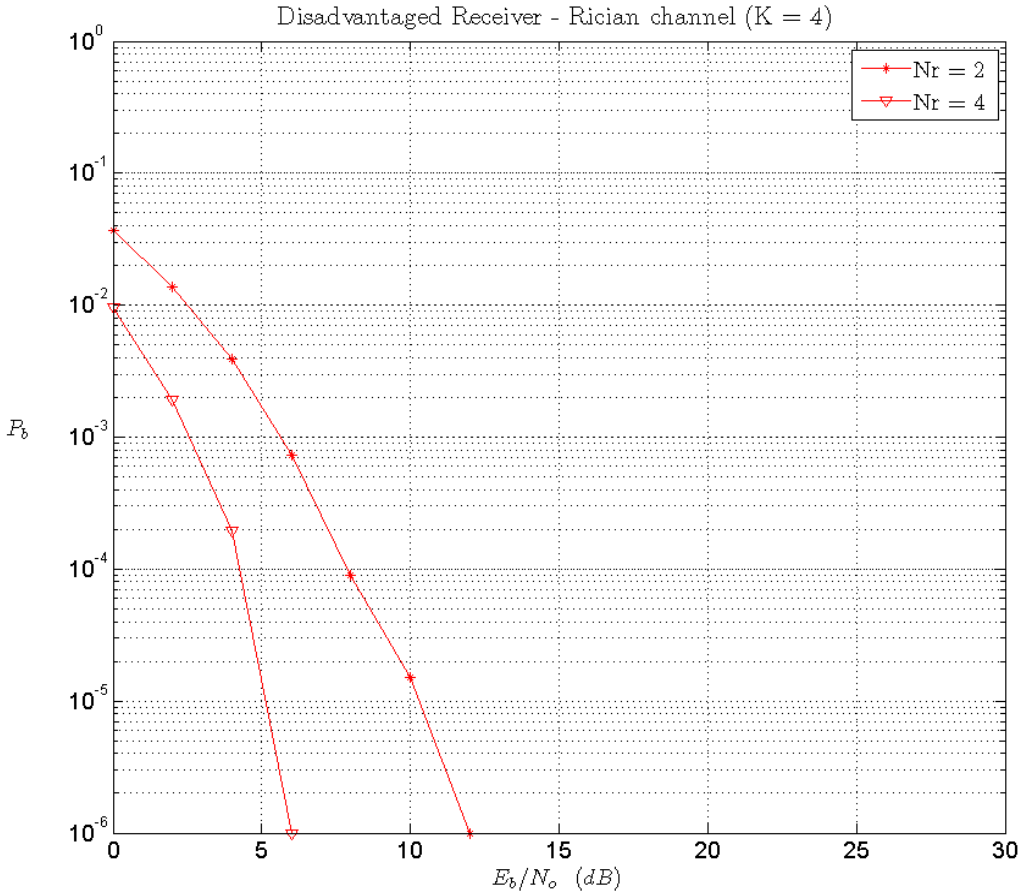

Figure 32. Simulated BER performance of the disadvantaged receiver in a Rician channel (K=4), for 2x2, 2x4, and 2x8 MIMO systems.

G. SUMMARY

Chapter III provided bit error rate analysis and simulation results of the concepts introduced in Chapter II. Simulation assumptions were presented and used throughout the chapter in an effort to provide for results that will be compared in the next chapter. The basic uncoded narrowband MIMO system was analyzed and simulated for numerous channel conditions as the basis for follow on analysis. Next, space time coding following the Alamouti scheme was refined and simulated. Then orthogonal frequency division multiplexing with space time coding was simulated. Channel state information was then incorporated into the narrowband system and simulated. Finally, the chapter concludes

with a situation in which a disadvantaged receiver was introduced to an existing system previously optimized for communication. Various results from these simulations are presented and compared in the next chapter.

THIS PAGE INTENTIONALLY LEFT BLANK

IV. COMPARISON AND RESULTS

This chapter compares the performance of the individual simulations presented the in last chapter. The comparison begins by investigating the performance of an uncoded system in Rayleigh and Rician channels. A space-time coded narrowband system is compared to an uncoded system. Then, narrowband performance is compared to that of OFDM. Next, the narrowband system is analyzed with and without channel state information. Finally, the performance of the primary receiver is compared to that of the disadvantaged receiver.

A. RAYLEIGH AND RICIAN CHANNEL MODEL COMPARISON

The discussion begins with an evaluation of the performance of an uncoded 2×2 MIMO system in Rayleigh and Rician fading channels. Figure 14. in Chapter III, section B, shows the performance of an uncoded MIMO system over Rayleigh and Rician fading channels. For this comparison QPSK was used, however, the results are similar for the other modulation schemes.

Recall from Chapter II, that the K - factor is a ratio of the power in the specular component (LOS) to that of the diffuse component (NLOS). Clearly, as the value of K increases, the specular component dominates and the channel approaches that of a non-fading channel or AWGN channel. This is confirmed by the increased performance of the system in a Rician channel to that of the Rayleigh channel. For a BER rate of 10^{-4}, a LOS component of equal power to that of the NLOS, as seen by the receiver, results in an improvement of 4.4 dB. Table 3. highlights the E_b/N_o required to achieve a particular BER.

Table 3. E_b/N_o required to achieve various BER for different channel models, 2x2 MIMO system with QPSK modulation.

BER	Rician (K=4)	Rician (K=1)	Rayleigh	Delta
10^{-3}	8.3 dB	11.2 dB	14.5 dB	*3.3 dB*
10^{-4}	10.6 dB	15.4 dB	19.8 dB	*4.4 dB*
10^{-5}	12.6 dB	19.5 dB	24.7 dB	*5.2 dB*
10^{-6}	14.8 dB	23.2 dB	30 dB	*6.8 dB*

Obviously, when the receiver has LOS to the transmitter, higher order modulation schemes may be employed and still achieve the same (or better) BER. Figure 33. compares QPSK, 16QAM and 64QAM with increasing power in the specular component. It is evident that beyond a BER of 10^{-4} the higher modulation schemes outperform QPSK due to the specular component. This implies that the specular component improves BER more than the higher order modulation degrades the BER.

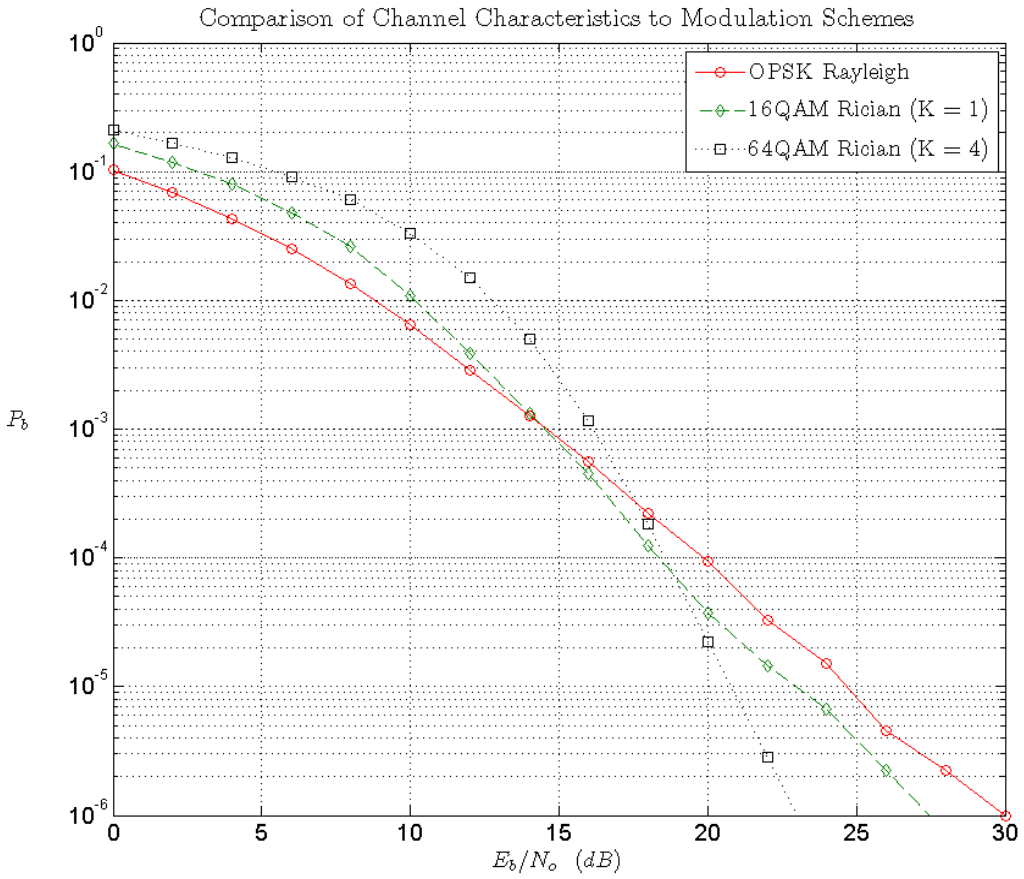

Figure 33. Simulated BER performance of various modulation schemes with different channel characteristics, 2x2 MIMO system.

B. UNCODED AND SPACE-TIME CODED COMPARISON

We now investigate the performance of an uncoded system to that of a space-time coded system. The Alamouti space-time code is designed to extract diversity when a minimum of two transmitting antennas are present, therefore we would expect to see a diversity gain when compared to the uncoded case. Figure 34. plots the BER performance of coded and uncoded QPSK in a Rayleigh channel.

The performance improvement seen the in plot is due to the diversity gain provided by the Alamouti scheme. Additionally, the orthogonality of the coding sequence transforms the decision at the receiver from a vector operation into a scalar

operation, reducing the receiver complexity. Comparing the required E_b/N_o to achieve a BER of 10^{-4}, we see that coding improves performance by 9.7 dB. Table 4. provides the required E_b/N_o to achieve a particular BER.

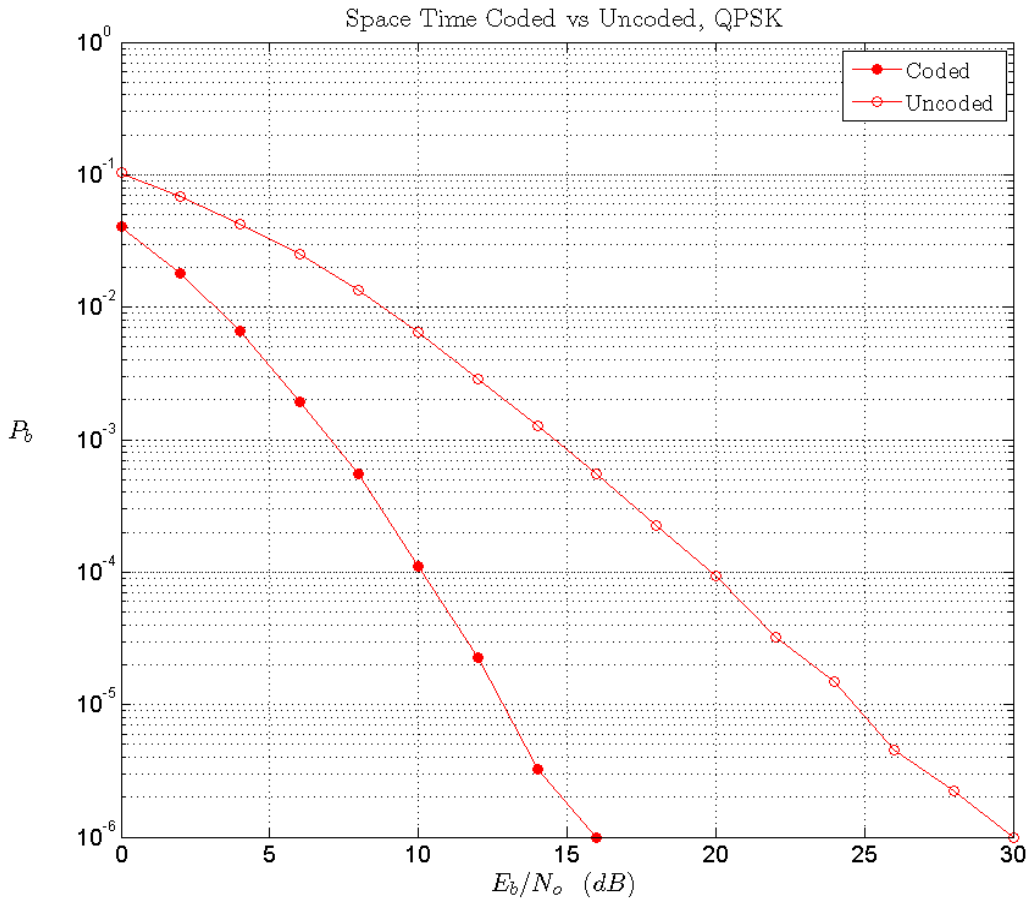

Figure 34. Simulated BER performance of uncoded and coded 2x2 MIMO system with QPSK modulation in a Rayleigh channel.

Table 4. E_b/N_o required to achieve a certain BER in a Rayleigh channel, 2x2 MIMO system using QPSK modulation, with and without Alamouti space-time coding.

BER	STC - Rayleigh	Rayleigh	Coding Gain
10^{-3}	14.5 dB	7.1 dB	*7.4 dB*
10^{-4}	19.8 dB	10.1 dB	*9.7 dB*
10^{-5}	24.7 dB	12.8 dB	*11.9 dB*
10^{-6}	30 dB	16 dB	*14 dB*

Next, we compare a coded system to an uncoded system characterized by a strong LOS component for all three modulation schemes, shown in Figure 35. It is interesting to see from the plot that an uncoded system over a Rician channel has a marginal improvement in performance past 12 dB (QPSK) to that of a space-time coded system. However, it is clear that a coded system outperforms an uncoded system even in an environment where the antenna has a dominate line of sight.

This demonstrates the advantage of antenna placement with respect to system performance, or if this is not possible the ability to apply the Alamouti scheme in order to improve performance. MIMO systems allow the system designer implement multiple techniques in order to establish robust communications. This simulation provides a comparison of the performance of these different techniques. As the simulation shows, Rayleigh fading degrades BER as compared to Rician fading with a strong LOS component (K = 4) roughly the same as uncoded compared to Alamouti coded.

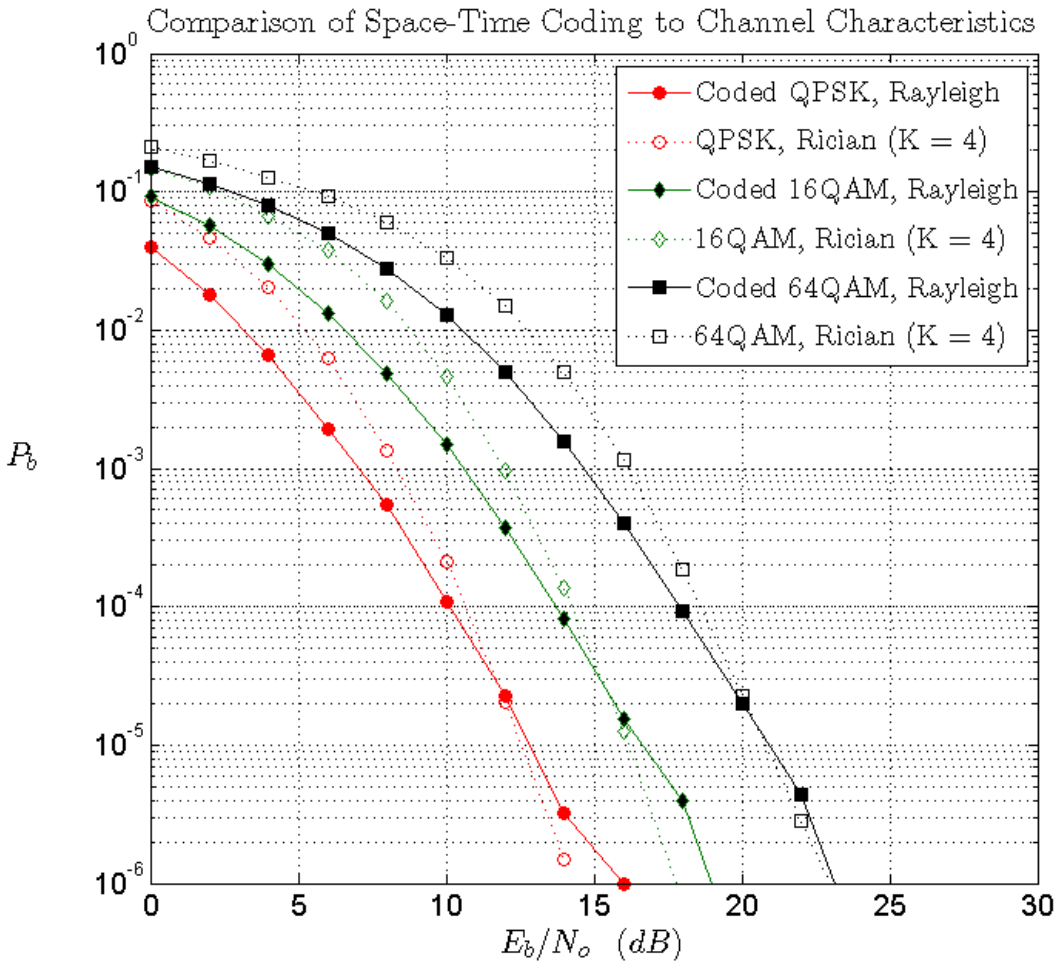

Figure 35. Simulated BER performance of a 2x2 MIMO system, various modulation schemes, uncoded and using Alamouti space-time coding, with different channel characteristics.

C. CODED NARROWBAND AND WIDEBAND COMPARISON

For this thesis, it was assumed that the channel provided slow frequency non-selective fading conditions. Thus, the performance of a coded wideband system will coincide with that of a narrowband system. Figure 36. confirms this result with a plot of BER for 64QAM with Alamouti space-time coded wideband and narrowband 2×2 MIMO system.

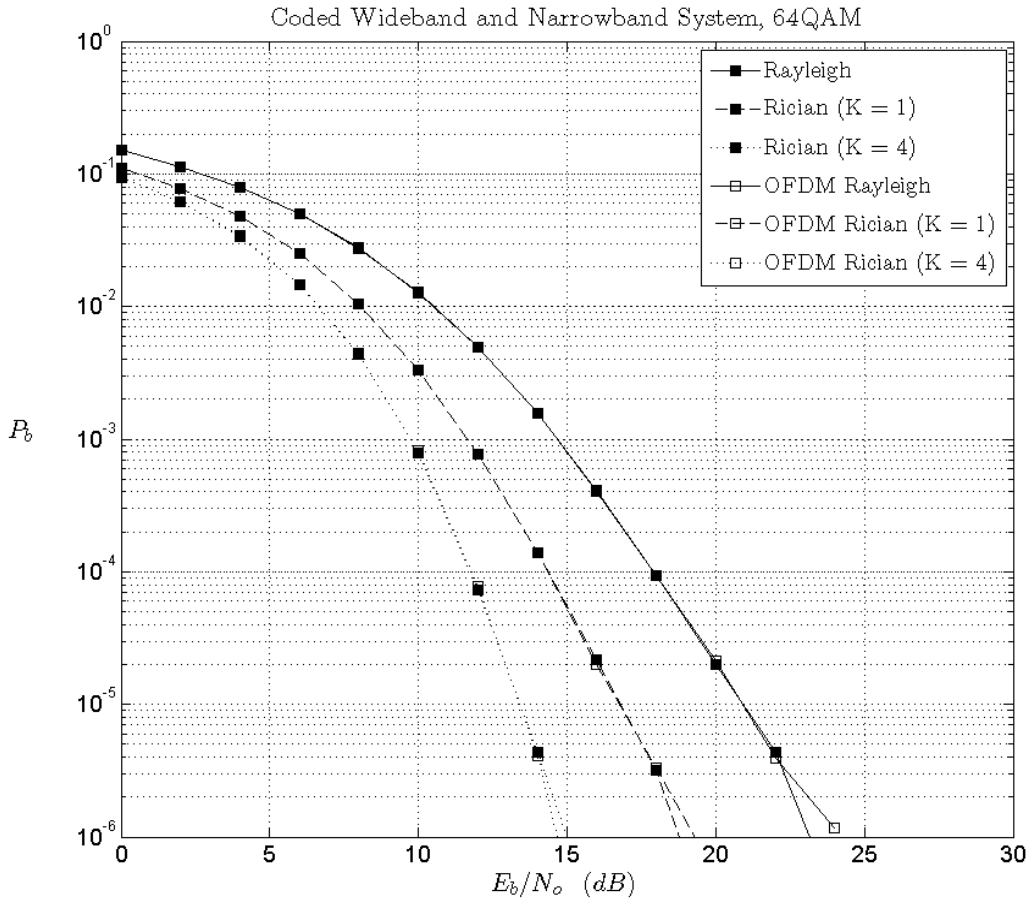

Figure 36. Simulated BER performance of a 2x2 MIMO system using Alamouti space-time coding, wideband and narrowband in various channels with 64QAM modulation.

D. TRANSMITTER WITH AND WITHOUT CSIT COMPARISON

In this section, the performance of a system when the transmitter has CSIT will be compared to a system without. With a closed loop system, the information available to the transmitter can be applied to improve performance in a number of areas, depending on the design of the system. In this thesis we focus on the ability of the transmitter to increase the received SNR through the use of dominant eigenmode transmission, where the result of this application is an array gain in addition to the diversity gain. Therefore, we expect that the performance increase over the uncoded case will be considerable.

Figure 37. plots the error rate performance of a 2×2 MIMO system with and without CSIT where both Rayleigh and Rician fading are considered. From the illustration it is clear that there is a significant improvement when the transmitter has knowledge of the channel. For a BER rate of 10^{-4}, the system with CSIT results in an improvement of roughly 12 dB. Table 5. highlights the E_b/N_o required to achieve a particular BER.

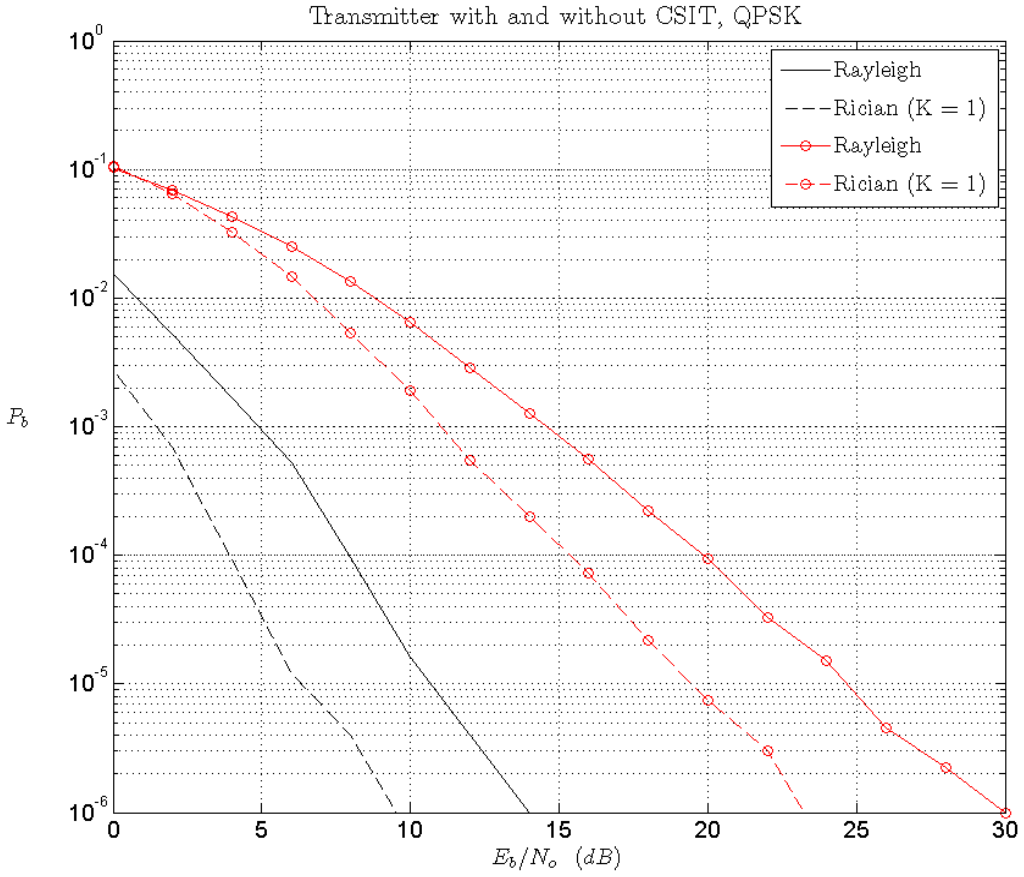

Figure 37. Simulated BER performance of a transmitter with and without CSIT for a 2x2 MIMO system in various channels using QPSK modulation.

Table 5. E_b/N_o required to achieve a BER in Rayleigh channel and Rician channels when the system has CSIT, 2x2 MIMO system.

BER	Rayleigh	CSIT Rayleigh	Delta	Rician	CSIT Rician	Delta
10^{-3}	14.5 dB	5 dB	*9.5 dB*	11.2 dB	1.4 dB	*9.8 dB*
10^{-4}	19.8 dB	7.9 dB	*11.9 dB*	15.4 dB	3.8 dB	*11.6 dB*
10^{-5}	24.7 dB	10.7 dB	*14 dB*	19.5 dB	6.3 dB	*13.2 dB*
10^{-6}	30 dB	14 dB	*16 dB*	23.2 dB	9.5 dB	*13.7 dB*

The performance trends displayed in Figure 37. are as expected; the array gain increases the BER of the entire system for all values of E_b/N_o, while the diversity gain improves BER performance for large values of E_b/N_o.

Figure 38. compares a system employing the Alamouti space-time code and no CSIT to a system with CSIT and no STC in Rayleigh fading. In this figure, it is clear that both systems offer the same diversity. However, the system employing CSIT shows a consistent improvement of 2 dB. This is due to an array gain resulting from the coherent combining of the precoded signals at the receiver. Thus, for the same diversity order we see that knowledge of the channel at the transmitter improves performance by 2 dB. Of course, this improvement in performance is at the cost of increased overhead due to the requirements of the feedback channel.

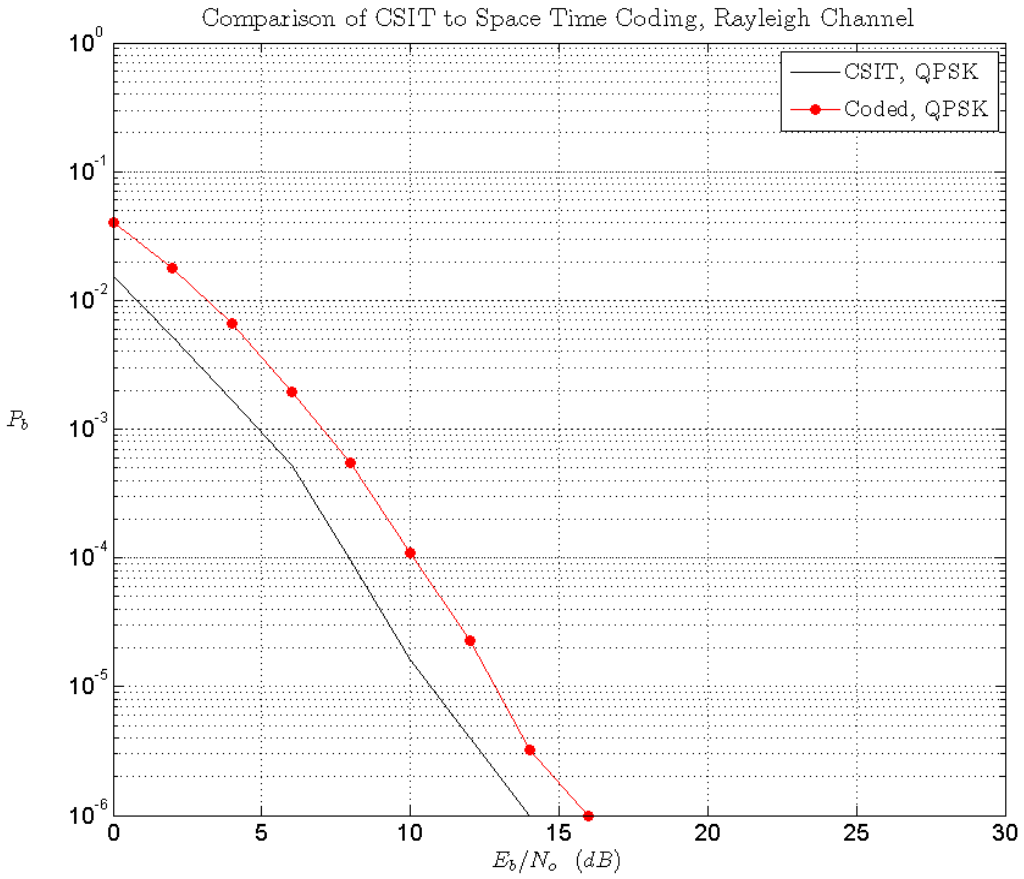

Figure 38. Simulated BER performance of a 2x2 MIMO system with CSIT to that of a system with Alamouti space-time coding both in a Rayleigh channel using QPSK modulation.

E. DISADVANTAGED RECEIVER COMPARISON

The results in this thesis illustrate that MIMO communications allow the system designer the ability to produce a system that specifically addresses the environment in which it operates. That is one of the benefits of MIMO communications. When a MIMO system is optimized using the techniques presented in this thesis, such as employing channel state information to overcome channel characteristics specific to that radio link, introducing a second receiver to the system could pose a serious problem, because that optimization is specific for the first receiver's channel gains.

In this final section, we investigate the performance of a receiver that is disadvantaged with respect to the intended receiver. That is, the disadvantaged receiver does not enjoy the same optimization of the transmission, as does the intended receiver. The goal of this comparison is to integrate the topics discussed previously in order to produce performance at the disadvantaged receiver that is equal if not better than that of the intended receiver.

Recall, the system in question, presented in the last chapter, shown in Figure 39.

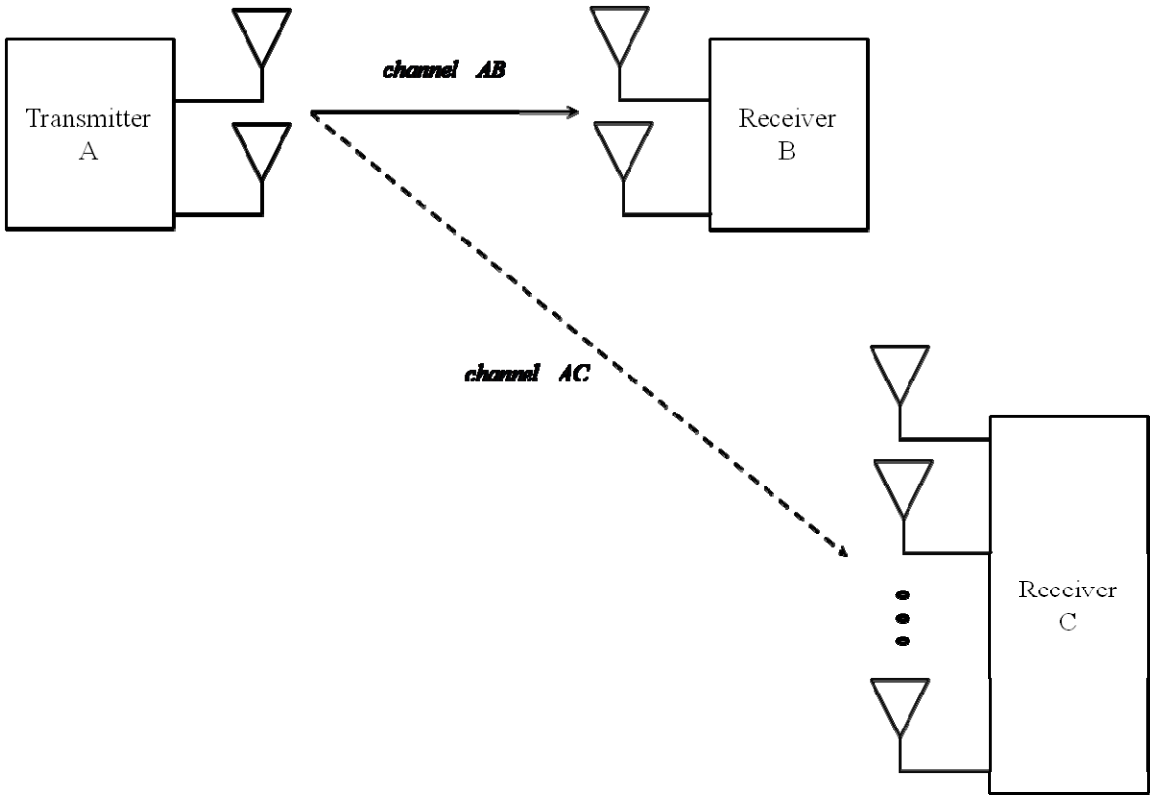

Figure 39. Disadvantaged receiver in a fixed MIMO system optimized for channel AB.

Transmitter A has channel state information of channel AB and uses dominate eigenmode transmission in order to improve the SNR at receiver B, the intended receiver. Consider receiver C, which is introduced to the system and does not enjoy the same optimization as the intended receiver, B.

1. Disadvantaged Receiver in a Rayleigh Channel

First, we compare the performance of both receivers in a Rayleigh channel, shown in Figure 40. The modulation for all systems in this section is QPSK.

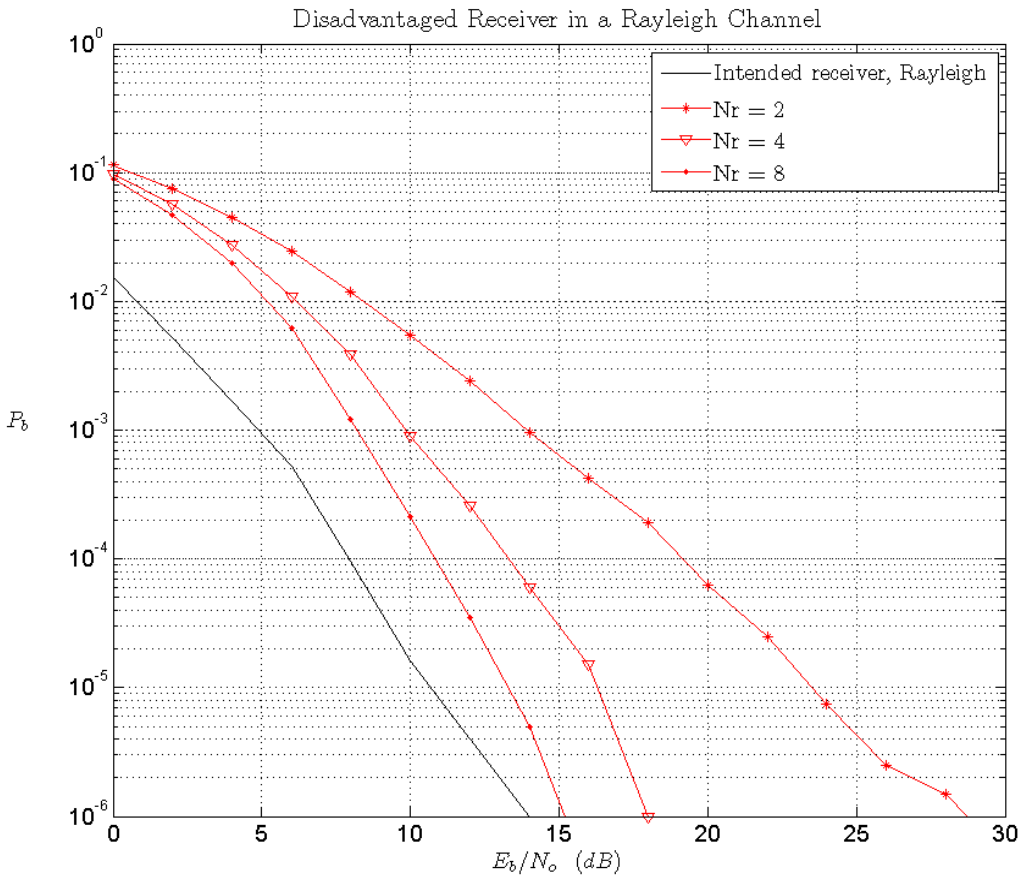

Figure 40. Simulated BER performance of a disadvantaged receiver in a fixed MIMO system, Rayleigh channel.

From the simulation results, it is clear that even when the disadvantaged receiver employs eight receive antennas, the performance is still worse than for the intended receiver. At a BER of 10^{-6} with eight receive antennas, the difference is 1.2 dB. However, depending on the application, this performance may prove to be adequate. Table 6. provides performance values for specific values of E_b/N_o.

Table 6. E_b/N_o comparison for select values of BER, disadvantaged receiver with various antenna configurations over a Rayleigh fading channel.

BER	Intended Rayleigh	Disadvantaged Rayleigh, Nr = 8	Delta
10^{-3}	5 dB	8.2 dB	*3.2 dB*
10^{-4}	7.9 dB	10.8 dB	*2.9 dB*
10^{-5}	10.7 dB	13.2 dB	*2.5 dB*
10^{-6}	14 dB	15.2 dB	*1.2 dB*

2. Disadvantaged Receiver in a Rician Channel (K = 1)

Next, we look at a situation in which receiver C has a LOS path to the transmitter. Where there is equal power in the specular and diffuse paths, shown in Figure 41.

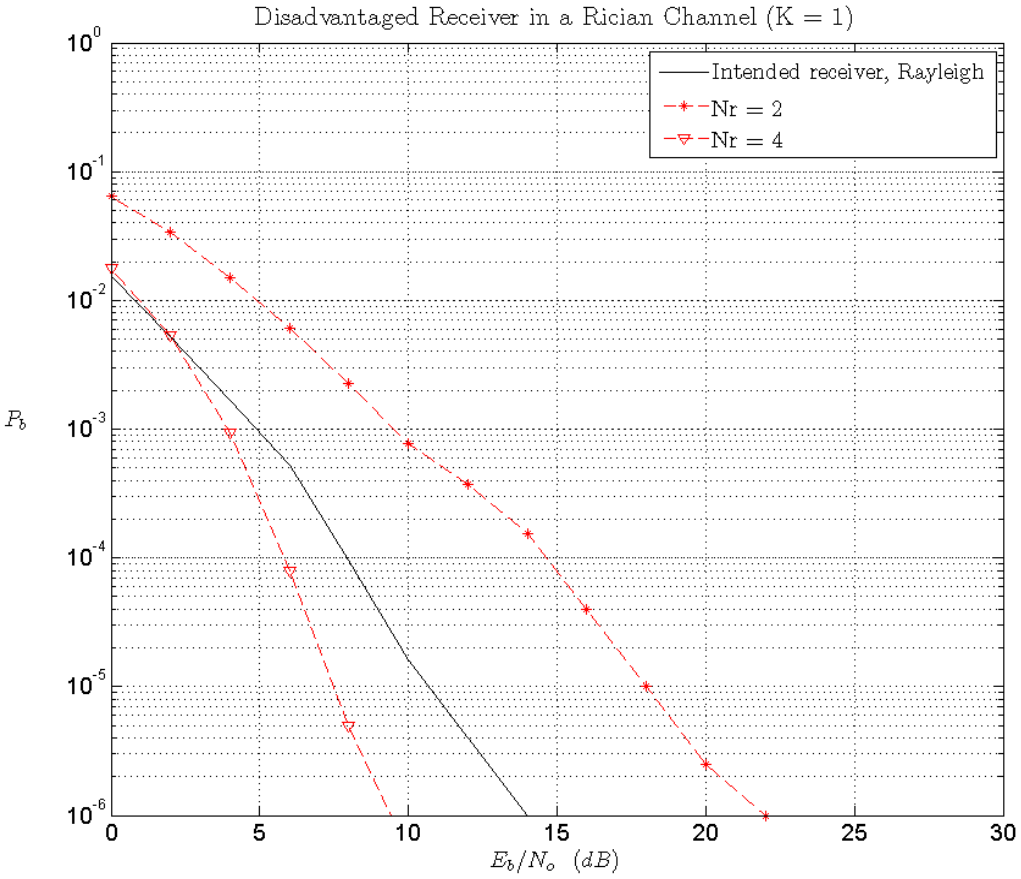

Figure 41. Simulated BER performance of a disadvantaged receiver in a fixed MIMO system, Rician channel (K = 1).

Clearly, performance is improved for receiver C compared to that of the Rayleigh case of Figure 40. , as expected. From the graph, we see that with two receive antennas performance still does not approach that of the intended receiver. However, when the number of antennas is doubled, the performance of receiver C is comparable at low values of E_b/N_o and provides superior performance at high values of E_b/N_o. Table 7. highlights this improvement.

Table 7. E_b/N_o comparison for select values of BER, disadvantaged receiver with various antenna configurations over a Rician channel (K = 1).

BER	Intended Rayleigh	Disadvantaged Rice, Nr = 4	Delta
10^{-3}	5 dB	3.9 dB	*1.1 dB*
10^{-4}	7.9 dB	5.8 dB	*2.1 dB*
10^{-5}	10.7 dB	7.5 dB	*3.2 dB*
10^{-6}	14 dB	9.4 dB	*4.6 dB*

3. Disadvantaged Receiver in a Rician Channel (K = 4)

Finally, we look at a situation in which receiver C has a more significant LOS path to the transmitter, illustrated in Figure 42.

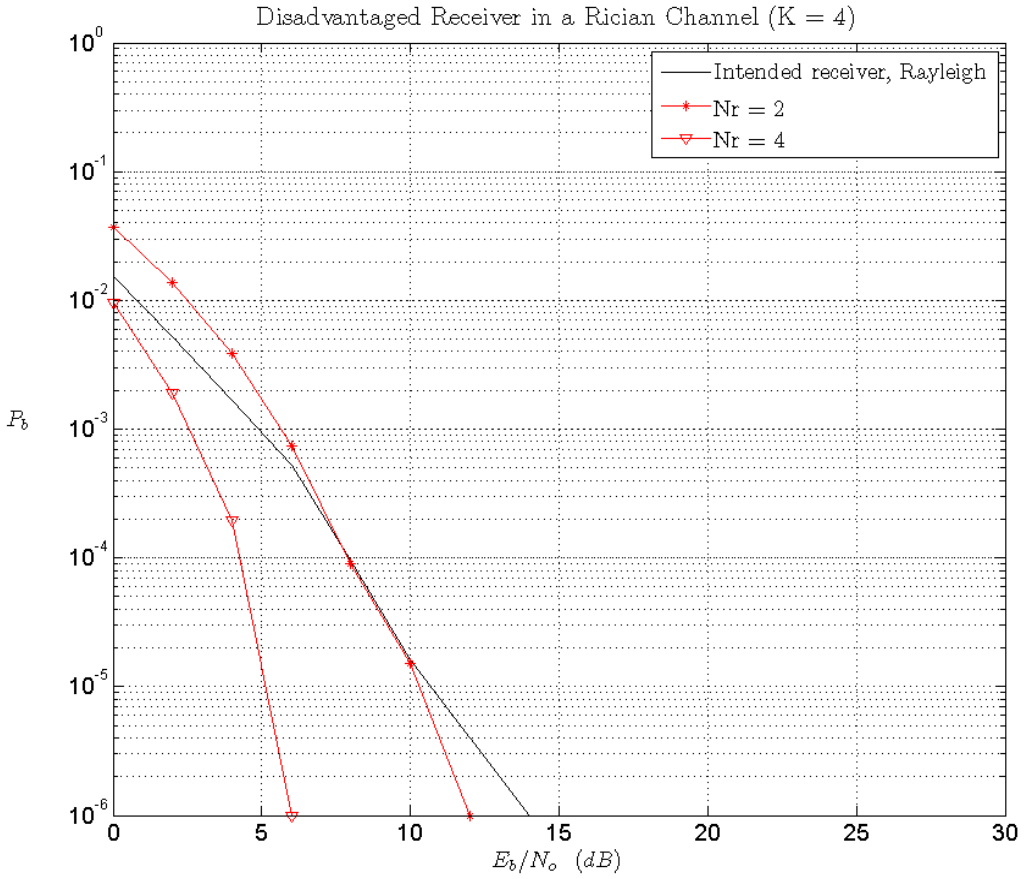

Figure 42. BER performance of a disadvantaged receiver in a fixed MIMO system, Rician channel (K = 4).

We observe that with two antennas, receiver C enjoys similar performance to the intended receiver. Obviously, four antennas provide an even greater performance gain. A transmitter with eight antennas was not evaluated since the result of four antennas is sufficient, but it is expected that BER performance increases dramatically as the number of antennas increases. Table 8. gives specific values for E_b/N_o.

Table 8. E_b/N_o comparison for select values of BER, disadvantaged receiver with various antenna configurations over a Rician channel (K = 1).

BER	Intended Rayleigh	Disadvantaged Rice, Nr = 4	Delta	Disadvantaged Rice, Nr = 2	Delta
10^{-3}	5 dB	2.5 dB	*2.5 dB*	5.6 dB	*0.6 dB*
10^{-4}	7.9 dB	4.2 dB	*3.7 dB*	7.8 dB	*0.1 dB*
10^{-5}	10.7 dB	5.1 dB	*5.6 dB*	10.3 dB	*0.4 dB*
10^{-6}	14 dB	6 dB	*8 dB*	12 dB	*6 dB*

When considering the performance of the disadvantaged receiver as the number receive antennas increased, recall from the first section in Chapter III, that the average total energy per bit received is equal to the transmitted energy per bit per transmit antenna by convention. In other words, both systems have the same total average E_b. As a result, increasing the number of receive antennas reduces the channel gains of the system. Thus, our assumption diminishes the performance gained by increasing the number of receive antennas at the disadvantaged receiver. Of course, if the systems had different E_b and N_o, those values would be used to make a more accurate comparison. The gross path loss, or geometry with respect to the transmitter, may favor one receiver over the other. In this case, we would see an even greater improvement in performance since the greater number of receive antennas results in more received power and thus a higher E_b.

However, with the assumptions of this thesis, the results of the simulations show that when the disadvantaged receiver has a weak E_b/N_o, increasing the number of receive antennas is one method to significantly decrease the bit error rate.

F. SUMMARY

In this chapter, several different scenarios are compared in terms of BER performance, based on the results of the previous chapter. The first comparison investigated the performance of an uncoded MIMO system over Rayleigh and Rician

channels. The resulting improvement in BER performance over a Rician channel was presented. Next, a space-time coded system was compared to an uncoded system, where the diversity gain provided by the Alamouti scheme was made apparent. Then, narrowband performance was compared to that of OFDM. Subsequently, a MIMO system was analyzed with and without channel state information. Finally, the performance of the primary receiver in a MIMO system is quantified and compared to the performance of a disadvantaged receiver. The disadvantaged receiver is then presented with various configurations in order to improve it BER performance. The next chapter concludes this thesis and provides a summary of results.

V. CONCLUSION

The goal of this research was to investigate disadvantaged receiver performance compared to the intended receiver in a MIMO system with the transmission optimized for the intended receiver. This was accomplished through a progressive development process from the simple uncoded MIMO system to one that employs channel state information at the transmitter. Once the final system was developed, a second, disadvantaged receiver was added and configured such that the BER performance matched or exceeded that of the intended receiver. Each system was simulated in MATLAB and the BER performance was determined and compared.

A. SUMMARY

A comprehensive study of MIMO systems and technologies was presented. Specifically, the BER performance of the transmitter and receiver in several cases was developed, to include space-time coding, OFDM, and channel state information at the transmitter. A second receiver was then introduced into the final system and the performance utilizing the discussed technologies was investigated.

The systems were designed and simulated in MATLAB for each case, over both Rayleigh and Rician fading channels. The results obtained were presented in the form of BER performance curves and compared against each other.

B. SIGNIFICANT RESULTS

The following results are provided by this thesis.

The BER performance of a MIMO system increases significantly when a LOS component is present. This is completely consistent with intuition developed from the study of SISO systems. When equal power is present in the specular and diffuse components (K = 1), an improvement of 6.8 dB was observed for a bit error rate of 10^{-6}. In addition, a system employing a higher order modulation scheme such as 64QAM over a Rician channel is able to achieve equal, if not better, performance than a system with

QPSK modulation over a Rayleigh channel. This comparison was made in order to quantify the advantage of a receiver in a Rician channel as compared to one in a Rayleigh channel. That is important in this work as that might be the case for the disadvantaged and intended receivers described in Chapter IV, section E.

In Chapter IV, section B, MIMO systems utilizing the Alamouti space-time code were observed to improve the BER performance by 14 dB at a bit error rate of 10^{-6} when compared to uncoded systems. Moreover, in high E_b/N_o regions, a system communicating over a Rician channel provided increased performance to that of a coded system over a Rayleigh channel. This comparison further demonstrates the advantage of antenna placement with respect to system performance. This relates to the situation of a disadvantaged receiver since the fixed system may be designed in such a way as to exploit this result. In other words, with MIMO systems there are multiple techniques that can be implemented in order to establish robust communications. This work primarily focused on the situation in which the transmitter utilized channel state information in order to establish a reliable system. However, understanding of such other techniques benefits the designer of the disadvantaged system as well.

When the transmitter utilizes channel state information to increase receiver diversity we observe a significant performance increase over a system that does not have CSIT. For a BER of 10^{-6}, an improvement of 13.7 dB was revealed. Additionally, it was observed that the system with CSIT provides an array gain of 2 dB when compared to the system without channel state information.

When a disadvantaged receiver is added to the system it is seen that the BER performance cannot match that of the intended receiver when both receivers experience Rayleigh fading, even when the number of reception antennas is increased to eight. However, when the disadvantaged receiver is located such that it has a line of sight component (Rician fading), we observe that performance increases significantly. In the case of equal LOS and NLOS components, a disadvantaged receiver with four reception antennas outperforms the intended receiver. When the disadvantaged receiver has a more

significant LOS component, similar performance to that of the intended receiver can be found with only two receive antennas at the disadvantaged receiver.

C. RECOMMENDATIONS FOR FUTURE WORK

Four areas have been identified for future work. First, this work assumes that the system is located in a fixed environment. However, a more realistic environment may be investigated by relaxing the channel assumptions to allow for frequency selective fading.

Second, the communication system can be further refined with a space-time coding scheme and OFDM. Due to the channel conditions assumed, this thesis developed a system that was single carrier and uncoded. If the first recommendation is applied, then the system can be integrated with those techniques and the disadvantaged receiver performance can then be determined under the new channel conditions. Of course, utilizing OFDM with the first recommendation will provide similar results to the flat fading conditions considered in this work, since each subcarrier experiences flat fading conditions even when transmitted through a frequency selective channel. However, a simulation can be conducted to confirm this result.

Third, in this thesis the focus was on bit error performance. Future work can analyze the system from an information theory standpoint. That is, focus on the capacity of the various systems and compare the capacity gains (or losses). For this, the channel state information at the transmitter can be utilized to increase capacity rather than improving the receiver BER as was used in this study.

Fourth, the simulations performed in this work discovered that as the number of receive antennas employed by the disadvantaged receiver increased, so did the BER performance. However, future work can identify the point of diminishing returns with respect to the number of receivers. At what point do the number of antennas and the corresponding complexity outweigh the performance improvement gained? Simulations involving an increased number of antennas can easily determine such a threshold.

THIS PAGE INTENTIONALLY LEFT BLANK

LIST OF REFERENCES

[1] J. G. Andrews, A. Ghosh, and R. Muhamed, *Fundamentals of WiMAX Understanding Broadband Wireless Networking*, Upper Saddle River, New Jersey: Prentice Hall, 2007.

[2] J. G. Proakis, and M. Salehi, *Digital Communications*, 5th ed. New York: McGraw-Hill, 2008.

[3] A. Goldsmith, *Wireless Communications*, Cambridge, United Kingdom: Cambridge University Press, 2005.

[4] B. Vucetic, and J. Yuan, *Space-Time Coding*, West Sussex, England: John Wiley & Sons, 2003.

[5] A. J. Paulraj, R. Nabar, and D. Gore, *Introduction to Space-Time Wireless Communications*, Cambridge, United Kingdom: Cambridge University Press, 2003.

[6] T. Ha, *Theory and Design of Digital Communication Systems*, Cambridge, United Kingcom: Cambridge University Press, 2010.

[7] T. S. Rappaport, *Wireless Communications: Fundamentals and Applications*, 2d ed., Upper Saddle River, New Jersey: Prentice Hall, 2002.

[8] D. Tse, and P. Viswanath, *Fundamentals of Wireless Communication*,Cambridge, United Kingdom: Cambridge University Press, 2005.

[9] C. W. Therrien, and M. Tummala, *Probability for Electrical and Computer Engineers*, Boca Raton, Florida: CRC Press LLC, 2004.

[10] R. Prasad, *OFDM for Wireless Communications Systems*, Boston, Massachusetts: Artech House, 2004.

[11] S. Sesia, I. Toufik, and M. Baker, *LTE - The UMTS Long Term Evolution*, West Sussex, England: John Wiley & Sons, 2009.

[12] B. Sklar, *Digital Communications Fundamentals and Applications*, 2d ed., Upper Saddle River, New Jersey: Prentice Hall, 2001.

[13] X. Zhu, and R. D. Murch, "Performance Analysis of Maximum Likelihood Detection in a MIMO Antenna System," *IEEE Transactions on Communications*, vol. 50, no. 2, pp. 187–191, February 2002.

[14] S. M. Alamouti, "A Simple Transmit Diversity Technique for Wireless Communications," *IEEE Journal on Select Areas in Communications*, vol. 16, no. 8, pp. 1451–1458, October 1998.

[15] P. J. Smith, L. M. Garth, and M. Shafi, "Performance Analysis of Multiple-Input Multiple-Output Singular Value Decomposition Transceivers During Fading and other Cell Interference," *Microwaves, Antennas & Propagation, IET* , vol.1, no.6, pp.1111–1119, Dec. 2007.

[16] C. Oestges, and B. Clerckx, *MIMO Wireless Communications: From Real-World Propagation to Space-Time Code Design*, Oxford, United Kingdom: Academic Press, 2007.

[17] G. H. Golub, and C. F. Van Loan, *Matrix Computations*, 3d ed. Baltimore, Maryland: The Johns Hopkins University Press, 1996.

[18] E. Teletar, “Capacity of Multi-antenna Gaussian Channels," AT&T Bell Labs Internal Technical Memo, June, 1995.

[19] F. Gray, “Pulse code communication,” March 17, 1953. U.S. patent no. 2,632,058.

[20] A. J. Paulraj, D. A. Gore, R. U. Nabar, and H. Bolcskei, “An Overview of MIMO Communications—A Key to Gigabit Wireless”, *Proceedings of The IEEE*, vol. 92, no. 2, pp. 198–217.

INITIAL DISTRIBUTION LIST

5. Defense Technical Information Center
Ft. Belvoir, Virginia

6. Dudley Knox Library
Naval Postgraduate School
Monterey, California

7. Chairman, Code EC
Department of Electrical and Computer Engineering
Naval Postgraduate School
Monterey, California

8. Associate Professor Frank Kragh, Code EC/Kh
Department of Electrical and Computer Engineering
Naval Postgraduate School
Monterey, California

9. Professor Tri Ha, Code EC/Ha
Department of Electrical and Computer Engineering
Naval Postgraduate School
Monterey, California

10. Professor Clark Robertson, Code EC/Rc
Department of Electrical and Computer Engineering
Naval Postgraduate School
Monterey, California

11. Professor Roberto Cristi, Code EC/Cx
Department of Electrical and Computer Engineering
Naval Postgraduate School
Monterey, California

12. Donna Miller
Naval Postgraduate School
Monterey, California

13. Marine Corps Representative
Naval Postgraduate School
Monterey, California

14. Director, Training and Education, MCCDC, Code C46
Quantico, Virginia

15. Director, Marine Corps Research Center, MCCDC, Code C40RC
Quantico, Virginia

16. Marine Corps Tactical Systems Support Activity (Attn: Operations Officer)
Camp Pendleton, California